An-Najah National University
Faculty of Graduate Studies

CYSTEINE-MODIFIED CELLULOSE NANOPARTICLES AS A CONTROLLED DELIVERY SYSTEM FOR THE ANTITUMORAL DRUG DOXORUBICIN

By
Motasem Azzam Ahmad Far

Supervisors
Prof. Othman Hamed
Prof. Mohyeddin Assali

This Thesis is Submitted in Partial Fulfillment of the Requirements for the Master of Degree of Chemistry, Faculty of Graduate Studies, An-Najah National University, Nablus, Palestine.

2026

CYSTEINE-MODIFIED CELLULOSE NANOPARTICLES AS A CONTROLLED DELIVERY SYSTEM FOR THE ANTITUMORAL DRUG DOXORUBICIN

By
Motasem Azzam Ahmad Far

This Thesis was Defended Successfully on 24/05/2026 and approved by:

Prof. Othman Hamed	othman hamed
Supervisor	Signature
Prof. Mohyeddin Assali	
Co-Supervisor	Signature
Dr. Orwa Houshia	
External Examiner	Signature
Prof. Nidal Jaradat	
Internal Examiner	Signature

Dedication

To my wife, the apple of my eyes, and the one who pushed me to my limits

Who showed me the way, with patience and love

A colleague, a fiancé, a wife, and, hopefully, the mother of my children

To my mother, who always believed in me

Your prayers and love were my crutch

To my father, who taught me how to be a man

To my future family

To Prof. Othman Hamed, who was a lighthouse for me

To the science

I dedicate this work.

Acknowledgements

Thank God, first and last, who granted me strength, guidance, and success to complete this work.

I thank my supervisors, Professor Othman Hamed and Professor Mohyeddin Assali, for providing the necessary guidance and direction in this project. Thanks are also extended to the faculty members of the department and the technical supervisors of the chemistry laboratories, especially Mr. Ameed Amirah, for providing continuous technical support and the necessary academic environment for my work. And I would also thank my wife, Shatha Madi, for her assistance and sincere support.

I would also like to extend my heartfelt thanks to the professors and colleagues at the University of Naples Federico II for providing the necessary guidance and direction in this project.

And to every individual and institution that contributed in any way to the success of this work.

Declaration

I, the undersigned, declare that I submitted the thesis entitled:

CYSTEINE-MODIFIED CELLULOSE NANOPARTICLES AS A CONTROLLED DELIVERY SYSTEM FOR THE ANTITUMORAL DRUG DOXORUBICIN

I declare that the work provided in this thesis, unless otherwise referenced, is my own work and has not been submitted elsewhere for any other degree or qualification.

Student's Name: Motasem Azzam Ahmad Far

Signature: 

Date: 24/5/2026

List of Contents

List of Tables

List of Figures

List of Abbreviations

Abbreviations	Meannings
ASR	Age-standardized rates
DS	Degree of substitution
DAC	Dialdehyde cellulose
TEMPO	2,2,6,6-Tetramethylpiperidine 1-oxyl
DDS	Drug delivery systems
GAPDH	Glyceraldehyde-3-phosphate dehydrogenase
pHi	pH intracellular
pHe	pH extracellular
TME	Acidic Tumor Microenvironment
PNIPAM	Poly(N-isopropyl acrylamide)
ROS	Reactive oxygen species
DOXO	Doxorubicin
CMC	Carboxymethyl cellulose
IEDDA	Bioorthogonal inverse electron demand Diels-Alder
CNFs	Cellulose nanofibers
CNCs	Cellulose nanocrystals
BNC	Bacterial nanocelluloses
TNF	Necrosis factor
PVP	Polyvinylpyrrolidone
QSDDS	Supersaturated drug delivery system
Q-SNEDDS	Self-nanoemulsifying drug delivery systems
NAC	N-acetylcysteine
PPD	p-Phenylenediamine
THF	Tetrahydrofuran
CGM	Culture growth medium
PBS	Phosphate-buffered saline
Cell-Mela	Cellulose-Melamine
DLS	Dynamic Light Scattering
Cell-Cys	Cellulose cysteine
Cell-PDA	Cellulose-p-phenylenediamine
Cell-HD	Cellulose hydrazone (Cell-HD)

List of Appendices

CYSTEINE-MODIFIED CELLULOSE NANOPARTICLES AS A CONTROLLED DELIVERY SYSTEM FOR THE ANTITUMORAL DRUG DOXORUBICIN

By
Motasem Azzam Ahmad Far
Supervisors
Prof. Othman Hamed
Prof. Mohyeddin Assali

Abstract

This study explores the development and characterization of pH-responsive drug delivery systems (DDS), starting from the modification of cellulose polymer for targeting cancer therapy. Activated microcrystalline cellulose with Lithium Chloride in dimethylacetamide LiCl/DMAc system and chemically modified by various reagents was synthesized. Modification includes the synthesis of cellulose tosylate and dialdehyde cellulose (Cell-A) as primary intermediates, then by substitution, these intermediates were functionalized with moieties such as L-cysteine, melamine, p-phenylenediamine, and hydrazine, introducing thiol, amine, and imine groups on the cellulose backbone to produce stable and specialized drug carriers. FT-IR and NMR spectroscopies confirmed successful modifications. Cellulose-cysteine (Cell-Cys) nanoparticles loaded with quercetin were prepared with a diameter of 70–90 nm and a zeta potential of -28 mV, showing strong electrostatic stability. The quercetin loading efficiency on the nanoparticles reached about 17.04%. A significant pH-dependent behavior was shown by the release studies on different carriers for both quercetin and doxorubicin (DOXO), for example, the quercetin released from Cell-Cys was 70 times more at pH 6.5 (tumor pH) than at the physiological pH (7.4). Cell-A and cellulose-hydrazone showed accelerated release of doxorubicin in acidic conditions, caused by the protonation of functional groups and increased polymer swelling. Cytotoxicity assays demonstrated that DOXO released from Cell-A maintained remarkable potency against HepG-2 cells with an IC50 of 0.0089 µg/ml, nearly identical to the free drug (0.0088 µg/ml). These findings lead to the conclusion that modified cellulose nanocarriers offer a biocompatible, stable, and highly efficient platform for the controlled and triggered release of anticancer agents.

Keywords : Cellulose, Cysteine-functionalized cellulose, Nanoparticles, Drug delivery system, Controlled drug release, pH-responsive release, Doxorubicin, Cancer therapy, Hydrazone linkage, Nanocarriers

Chapter One

Introduction

1.1 Cancer

1.1.1 Cancer types and causes

Cancer was and is still the leading cause of morbidity and mortality worldwide. And the recent research showed that cancer incidence worldwide for both sexes, corresponding age-standardized rates (ASR) in 2022, was approximately 18.74 million cases, such as lung cancer, which is the most common type of cancer, with 1.57 million incidences and 1.23 million deaths out of the 1.57 million [1], so there was a need for a treatment for this disease, which is caused by gene mutations at the tissue level, where it varies according to the type of tissues that are affected by this abnormal growth of tissues, causing a tumor that invades the surrounding tissues, posing a serious challenge in treating cancer [2].

Cancer incidence rate in the twentieth century witnessed a noticeable increase due to the overlap of lifestyle factors, while smoking and alcohol consumption are two of the most important contributors to lung and liver cancer[3], diabetes and lack of physical activities, other factors increasing the incidence rate and cancer-related deaths, as well as about 2% - 3%[4]. Recent studies have provided evidence that exposure to environmental carcinogens, such as viruses, polluted air, pesticides, dioxins, and persistent organic pollutants, is a major factor in carcinogenesis [5, 6], alongside genetic susceptibility and aging-related vulnerabilities [7].

The definition of cancer extended to a group of diseases caused by uncontrolled cell proliferation and the ability to attack other parts of the body. The main reasons for the development of cancer involve environmental exposures, genetic mutations, and disruptions in cellular signaling pathways, leading to tumor progression [8, 9]. There are many types of cancer, which are classified by tissue of origin, histological features, and molecular and genetic profiles [8]. Numerous traditional treatment methods, such as chemotherapy, surgery, radiation therapy, and hormonal therapy, each of these methods has its own mechanisms and challenges [8]. The centerpiece of cancer treatment is chemotherapy because of its rapid targeting of cancer cells, but it faces some challenges, including drug resistance and side effects [9]. To improve specificity and reduce toxicity,

recent research has introduced immunotherapies, targeted therapies, and novel drug-delivery systems [9].

1.1.2 Mechanisms of Cancer Development

Factors such as epigenetic changes, genetic mutations, and environmental factors that disrupt cell cycle regulation, leading to uncontrolled proliferation and resistance to apoptosis. resistance to cell death, angiogenesis, metastasis, invasion, and sustained proliferative signaling.

A main reason for the development of cancer is genetic mutation, which includes oncogene activation and tumor suppressor loss, which initiate clonal expansion, but also depends on epigenetic reprogramming, interactions with the tumor microenvironment, and chromatin remodeling. Summing these up together leads to tumor evolution. Epigenetic changes can increase cellular plasticity, endowing tumor tissues with a novel characteristic that enables cancer cells to evade normal controls and form malignant tissues [8, 10].

Another mechanism used by cancer to boost tumor initiation and progression is Inflammation within the tumor microenvironment, which supports cancer cell survival, metastasis, and growth, functioning like the tissue repair and immune systems [10].

1.1.3 Types and Classification of Cancer

Cancer classification usually depends on tissue or organ, molecular, and genetic profiles, as well as histological features. 200 cancer types and subtypes have been classified using machine learning approaches on comprehensive genomic profiling. On a histological scale, cancer can be categorized into major groups, including:

- Carcinomas are the most common type of cancer that invades epithelial cells.
- Sarcomas: rare types of cancer happen in connective tissues such as muscles, bones, and blood vessels.
- Leukemias: cancers that affect the bone marrow, blood, and lymphatic system, characterized by the rapid, uncontrolled production of white blood cells.
- Lymphomas: blood cancer developed in the lymphatic system.

- Myeloma: a blood cancer that occurs in abnormal plasma cells in the bone marrow, causing bone damage.
- Adenocarcinomas: a common type of cancer that attacks glandular epithelial cells, which are responsible for producing and releasing chemicals such as hormones and mucus.
- Blastomas: a group of malignant tumors primarily affecting children

1.1.4 Tumour cell pH

Cancer cells live in a pH gradient: the surrounding environment is slightly acidic, while the inner environment is slightly neutral or basic. And this difference between cancer cells and healthy cells was the key target for drug delivery, diagnostics, and immunotherapy. The question is, why do tumours have this pH pattern?

Firstly, the Warburg effect, in which cancer cells preferentially use glycolysis to break down glucose into lactate, enables them to rapidly produce biomass. Producing excess lactic acid (lactate + H^+), protons can also be produced as a byproduct of glycolytic enzymes like glyceraldehyde-3-phosphate dehydrogenase (GAPDH), and proton pumps export these protons to acidify the extracellular space for survival and growth [11]. Secondly, Poor vasculature and weak blood flow prevent acid washout, deepening local acidosis [12].

In tumors, pH gradients from external to internal, as measured by nano-sensor imaging, show spots with pH less than 5.3 adjacent to cancer cell membranes due to focused proton–lactate export [13]. Brain glioma models have a pH intracellular (pHi) ~ 7.4, while the extracellular pH (pHe) is ~ 6.6-6.8 [14]. The acidic pH values stimulate metastasis, invasion, extracellular Matrix (ECM) degradation, and drug resistance [15], Alkaline pHi supports survival and proliferation [16]. The acidic Tumor Microenvironment (TME) inhibits T-cell and NK-cell function, weakening immunotherapy.

1.2 Chemotherapy

Cytotoxic drugs are a type of drug that is used to kill or control cancer cells in the body, through different types of mechanisms focusing on DNA or cell division machinery [17]:

- Alkylating agents and platinum drugs create inter- and intra-strand crosslinks with DNA and block replication, leading to death.
- Antimetabolites: simulate natural metabolites and interfere with DNA and RNA synthesis.
- Topoisomerase inhibitors: stop cancer cells' growth by misfunctioning topoisomerase I or II enzymes
- Mitotic (microtubule) inhibitors: interrupt cell division by connecting to tubulin to block the assembly of the mitotic spindle.

1.2.1 Combination with other therapies

Chemotherapy drugs are usually combined with other techniques to get the most benefits from them, such as multi-drug chemotherapy, which often exceeds the use of a single agent. For example, combining methotrexate, cisplatin, ifosfamide, and doxorubicin improves survival in osteosarcoma. Some techniques combine chemotherapy drugs with immunotherapy. Cytotoxic agents can enhance responses to checkpoint inhibitors and make tumor cells more visible to the immune system, thereby increasing immunogenic cell death. Such as the addition of immunotherapy to chemotherapy drugs based on platinum, which adds an acceptable toxicity, but improves overall survival in lung and small-cell lung cancer. Nanocarriers combined with chemotherapy drugs also maximize the cytotoxic effect by concentrating the drugs in the tumor, boosting efficacy, and reducing systemic toxicity. Combining natural compounds with chemotherapy is also one of the techniques that can be used in this case, such as polyphenols, which may discover tumors, overcome resistance, and reduce side effects in preclinical models [18, 19].

1.2.2 Benefits of chemotherapy

Chemotherapy with a wide range of cytotoxics is still the cornerstone of cancer treatment; despite its known side effects, it is still used to treat some types of cancer, reducing the symptoms, and sometimes alongside other types of cancer treatments such as surgery, radiotherapy, or immune therapies.

1.2.3 Mechanisms and Indirect Benefits

By interfering with DNA and cell division, it causes direct tumor killing and tumor shrinkage, with a preference for killing rapidly dividing cancer cells. Another strategy used is enabling a combination with other therapies, which helps the immune system to recognize cancer cells and make them more visible to the immune system [9].

1.2.4 New anti-tumor drug

In recent years, numerous anti-tumor agents, particularly nanocarrier-based systems, have been developed, broadening the spectrum of cancer treatments. These innovations enhance the efficacy of anti-tumor drugs, gene therapies, immunotherapies, and RNA interference therapies, while simultaneously reducing adverse effects.

Currently, traditional chemotherapy agents are categorized into seven groups: (1) compounds that disrupt DNA structure and function, such as nitrogen mustard, etilican, cisplatin, and bleomycin; (2) agents inhibiting nucleic acid biosynthesis, including fluorouracil, methotrexate, and gemcitabine; (3) drugs interfering with transcription and RNA synthesis, such as epirubicin and doxorubicin; (4) inhibitors of protein synthesis, for example vinblastine and paclitaxel; (5) modulators of hormonal pathways such as megestrol, tamoxifen, fulvestrant, and exemestane; (6) molecular targeted agents, including trastuzumab, imatinib, and sunitinib. These anticancer medications can be administered via various routes, including injection, oral administration, subcutaneous implantation, intravenous infusion, and localized delivery, depending on the treatment protocol and specific drug characteristics.

Chemotherapy drugs destroy tumor cells but also harm normal cells, causing side effects. These medications target rapidly dividing cells indiscriminately, leading to toxic effects on blood-forming cells, hair follicles, and intestinal mucosa. As a result, patients may experience anemia, vomiting, nausea, diarrhea, and hair loss [20]. Additionally, chemotherapy suppresses the immune system, raising the risk of infections such as cystitis, which may require antibiotics [21]. Additionally, other side effects include extreme exhaustion, which could be caused by the psychological stress of treatment, as well as the toxicity of the medication [20]. Symptoms can be noticed, such as vomiting and nausea, and weight loss is common due to decreased appetite, leading to malnutrition [21]. Otherwise, nephrotoxicity, ototoxicity, and hepatotoxicity seem not to be

exceptional. Some medications can cause hearing loss and impair kidney and liver function [24]. Certain chemotherapies may lead to neurological issues like paresthesia, peripheral neuropathy, and limb weakness. Other side effects include fertility problems, cardiotoxicity, and sexual toxicity, with many lasting years and impacting the patient's quality of life.

Drug resistance poses a major challenge to chemotherapy, often leading to treatment failure due to varying tumor sensitivity to drugs [25]. Chemotherapy drug resistance can be intrinsic or acquired. Epigenetic changes largely drive intrinsic resistance, while acquired resistance develops gradually during long-term drug exposure. Mechanisms behind acquired resistance include: (1) reduced drug uptake; (2) diminished drug accumulation in tumor cells; (3) altered activity of drug-inactivating enzymes; (4) decreased substrate availability for drug action; (5) increased drug efflux; (6) enhanced DNA repair in tumor cells; and (7) activation of alternative metabolic pathways.

Chemotherapy also has so many disadvantages, such as high cost, high toxicity, risks of infection, pain from injections, and differences in individualized treatment responses [22]. These reasons cause side effects that are very harmful to the human body. So, there is an eagerness to improve anticancer drugs that reduce side effects without minimizing their efficacy. To overcome these challenges, researchers developed new anti-tumor drugs and dosage forms.

1.2.5 Anticancer drug carriers

Recent developments in nanocarriers, such as self-assembled nanomedicine combined with berberine derivatives and doxorubicin, have shown that they can enhance anti-metastatic and anti-tumor effects by acting through mitochondrial pathways. Research has demonstrated that these drug-loaded nanocarriers can inhibit tumor cell growth and prevent lung metastasis[27]. Another example involves oral delivery of paclitaxel using D-alpha-tocopherol polyethylene glycol 1000 succinate (TPGS) modified carboxymethyl chitosan rhodopsinin (TCR) polymer micelles. These micelles have been found to increase the oral bioavailability of paclitaxel.[28] Figure 1 presents a basic classification of these nanocarriers, while Table 1 lists FDA-approved nanomedicines.

Nanocarriers generally enhance the effectiveness of chemotherapy and improve drug stability. Nonetheless, issues such as elevated costs, safety concerns, and potential toxicity persist, underscoring the need for continued research to optimize their application.

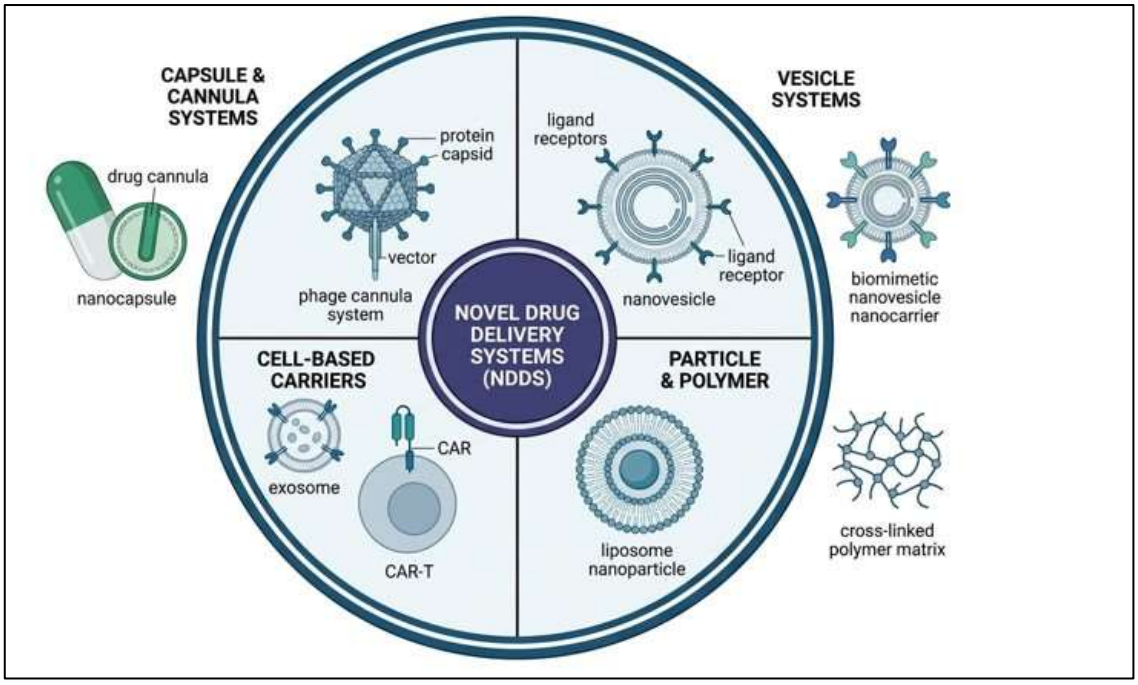

Figure 1*: The figure shows a summary of the types of nano-drug delivery systems*

Table 1*: Cancer drug carriers approved by the FDA*

Nanomedicine	Type	Therapeutic Use
Doxil	Liposome	Cancer (ovarian, multiple myeloma, etc.)
Abraxane	Nanoparticle-bound albumin	Breast, pancreatic, NSCLC
Onivyde	Liposome	Pancreatic cancer
Vyxeos	Liposome	Acute myeloid leukemia (AML)
Marqibo	Liposome	Acute lymphoblastic leukemia
DepoCyt	Liposome	Neoplastic meningitis

1.2.6 Slow and controlled release formulations of nanocarriers

Recent research has shown the significant role of slow-release formulations of anticancer drugs. Offering sustained drug release, reducing drug dosage, improving therapeutic efficacy, providing more convenient treatment regimens, and minimizing toxicity. In addition, slow-release systems are not significantly affected by factors such as enzymes, pH, and gastrointestinal motility. The gradual release of the anti-tumor drug into the body

maintains a stable effective blood concentration over an extended period [23]. Typically, the release of the drugs follows Higuchi diffusion kinetics or first-order. Systematic chemotherapy commonly uses intravenous injections, which may cause adverse effects on healthy cells, including repeated injections, pain at the injection site, the need for hospitalization, and potential infections [24]. Nanotechnology also has an impact on the mechanism of drug release. This can help reduce injection times, reduce the toxic effects on healthy tissues, and enhance the drug's efficacy, thus enhancing the patient's mood [25]. The benefits of slow-release systems can be gathered as follows (1): reduced injection number, which leads to enhanced patient compliance. (2): Stable drug concentration, by preserving blood drug levels and avoiding troughs and peaks, which decreases side effects (3). Optimized therapeutic effects (4). Adapted release, where the drug can be timed and targeted, making the formulation disease-specific. Examples of nanocarriers are shown in Figure 2.

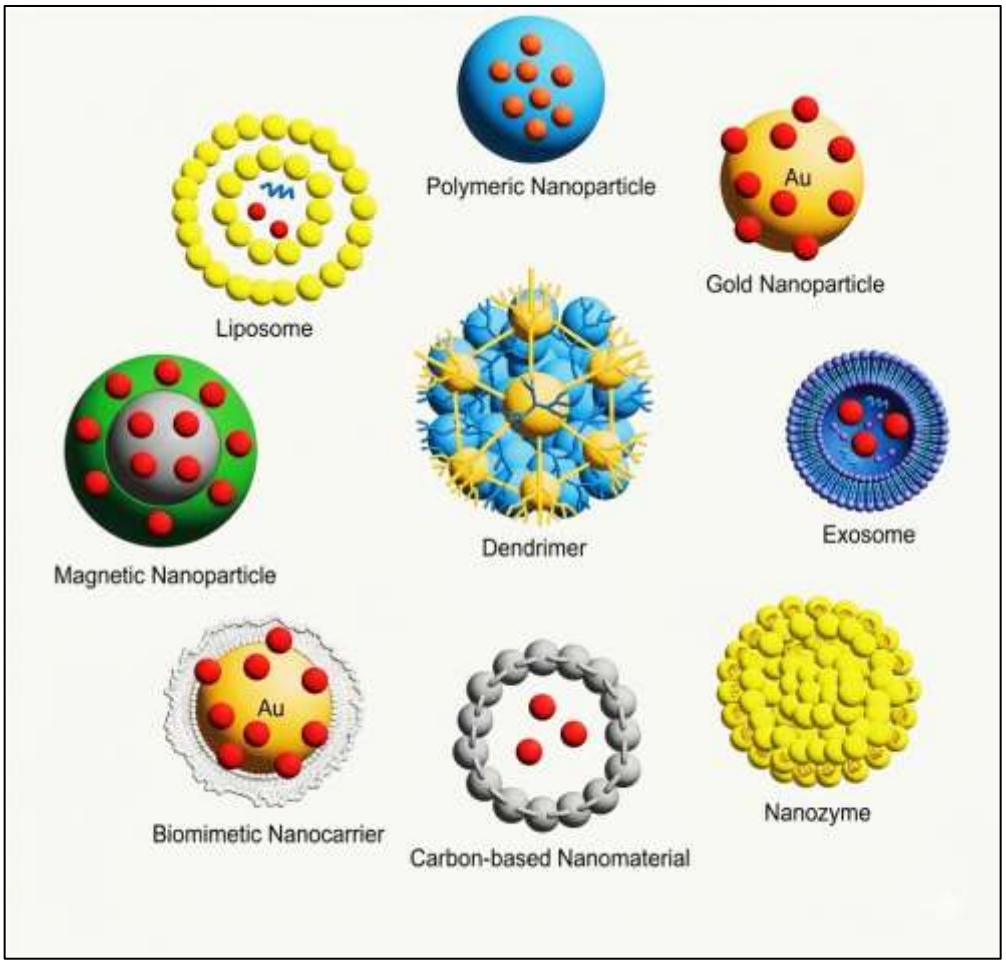

Figure 2: *Examples of anticancer drug nanocarriers.*

In this research, we are primarily concerned with polymer nanoparticles; examples are shown below. Dextran, Polylactic acid (PLA), Poly(lactic-co-glycolic acid) (PLGA), gelatin, poly(1,3-bis-(p-carboxyphenoxypropane)-co-(sebacic anhydride) (PCPP-SA), polycaprolactone (PCL), polyethylene glycol (PEG), chitosan, hyaluronic acid, and alginate.

Cellulose is another promising biopolymer that can be used, before or after modification, as a nanocarrier for drug delivery.

1.3 Cellulose

Cellulose, the most available natural polymer, can be extracted from many sources, including cotton plants, bacteria, and wood [26]. It is an important component of the cell wall of green plants. It is a polymer consisting of a repeating unit of D-glucose linked together by β-1,4 glycosidic bonds after losing water molecules to form a long and linear chain. Each anhydroglucose unit contains three hydroxyl groups, two of which are secondary, located on C2 and C3, and the other one is primary, located on C6, as shown in Figure 3. As we can see in the structure of cellulose, it is participating in an extensive network of hydrogen bonds within the polymer, and with the adjacent cellulose chains, there are four different types of cellulose: Type I, II, III, and IV [26].

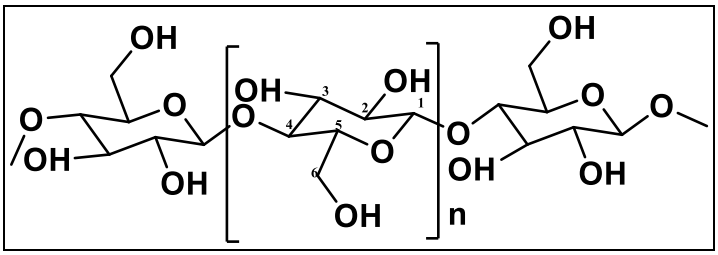

Figure 3*: Typical structure of a cellulose polymer.*

The process of forming the polymorphic Cellulose II from the naturally occurring Cellulose polymorphic (Cellulose I) is called mercerization, in which Cellulose I is allowed to dissolve in an alkaline medium (18% by mass NaOH) [27]. This causes the swelling of the cellulose due to the disruption of the hydrogen bonds because of the electrostatic repulsions. The addition of liquid ammonia to Cellulose I or II leads to the formation of Cellulose III after the treatment with 2,2,6,6-Tetramethylpiperidine 1-oxyl (TEMPO) [28]. The treatment of cellulose III with glycerol at high temperature converted it to cellulose IV [29].

Due to its biodegradability, biocompatibility, and non-toxicity, cellulose is considered highly valued for its safety, enabling its use in various biomedical applications [30]. Its chemical structure makes modification and conjugation with other materials feasible, leading to specific properties for applications such as tissue engineering, wound healing, bone regeneration, and drug delivery [31]. Bacterial cellulose offers exceptional mechanical strength and a porous structure to support cell growth, making it good for applications such as artificial skin, wound dressing, and vascular grafts [30, 32].

1.3.1 Modifications of cellulose

The chemical structure of cellulose, characterized by a high number of hydroxyl groups, forms hydrogen bonds within the polymer, resulting in a self-assembly structure, making it insoluble in a wide range of solvents [33], which restricts its ability to form suitable carrier structures, making it less flexible for encapsulating and delivering drug compounds. Hence, the improvement of processability and applicability of cellulose is achieved by the chemical modification of some or all of the hydroxyl groups. The hydroxyl groups can be modified by one of these reactions: esterification, etherification, or oxidation.

1.3.1.1 Etherification of cellulose

Generally, the reaction of cellulose with alkyl sulfates and alkyl chlorides leads to the esterification of cellulose on one or more of its hydroxyl groups, making the cellulose ether. And the effect of this reaction on the solubility depends on the degree of substitution (DS). Etherification is usually carried out in alkaline conditions to activate the hydroxyl groups on cellulose. A recent study reported an efficient method using tetra-n-butylphosphonium hydroxide in aqueous solution for rapid, mild etherification reactions [34]. Another study used mercerized cellulose with NaOH, followed by etherification with chloroacetic acid for several hours at 50-55 °C [35, 36]. Cellulose ethers can be used across many fields, including pharmaceuticals, personal care products, construction materials, and paints, due to their water solubility and viscosity-enhancing properties [37].

1.3.1.2 Esterification of cellulose

Cellulose esters are primarily prepared through an esterification reaction that converts the hydroxyl groups into esters. Cellulose esterification can be performed using a wide range of methods, including heterogeneous and homogeneous reactions, and the reaction type determines the DS and the reaction location, whether on the whole polymer or only on the surface [38]. A recent study used a green approach with carbocyclic acid-based deep eutectic solvents, which swell cellulose and esterify it, yielding a high yield of nanofibers, and preserving crystallinity [39]. But the reaction of vinyl esters with cellulose at room temperature in aqueous media. And the reaction of cellulose with p-toluenesulfonyl chloride forms cellulose tosylates, converting the hydroxyl groups to tosylate esters. This process utilizes solvents such as DMAc/LiCl or NaOH-urea as eco-friendly media, along with triethylamine. And the tosyl group serves as a good leaving group, allowing for further nucleophilic substitution reactions on cellulose.

1.3.1.3 Oxidation of cellulose

The modification of the cellulose hydroxyl group by an oxidizing agent typically converts it to a carboxyl or an aldehyde group, depending on the oxidizing agent. This enhances the functionality of cellulose for various applications, such as pharmacy, medicine, and nanomaterials fabrication [40]. There are many oxidation methods, including the use of nitrogen dioxide, permanganates, sodium nitrite combined with strong acids, ozone, lead (IV) tetraacetate, and sodium periodate; the latter two produce dialdehyde cellulose, which can be used for further applications and modifications [41, 42]. Additionally, TEMPO can be used to selectively oxidize the C6 primary hydroxyl group to carboxylates under mild aqueous conditions. D. Mendoza and his colleagues combined TEMPO with sodium periodate in a one-shot reaction to produce a highly carboxylated cellulose with controlled properties [43].

Sodium periodate selectively cleaves the C2-C3 bond, converting the two vicinal diols into a dialdehyde and producing dialdehyde cellulose (DAC), as shown in the scheme below (Figure 4). Temperature, in this case, has a stronger effect on the oxidation rate than the sodium periodate concentration, but it can cause some cellulose degradation at high temperature [44]. Juho Sirvio and his partners studied the effect of adding metal salts, such as lithium chloride, on the aldehyde content and showed that adding LiCl

enhances the reaction [45]. Treating cellulose with alkali and electrochemical assistance before the oxidation reaction can increase aldehyde content and alter crystallinity, thereby improving solubility and swelling [46].

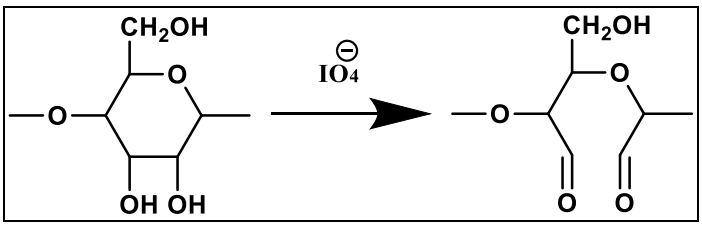

Figure 4*: The oxidation reaction of cellulose to DAC.*

1.3.1.4 Grafting cellulose polymers

Cellulose and modified cellulose can be grafted to improve drug loading and release. Ethyl cellulose has been grafted with polyethylene glycol (PEG) to form copolymers that self-assemble into micelles that can deliver Doxorubicin (DOXO) to cancer cells. And also, it is pH responsive, which releases DOXO under acidic environments [47]. Cellulose was similarly grafted with polylactic acid functionalized with targeting antibodies, thereby improving drug loading, targeted delivery, and antitumor efficacy in vitro and in vivo [48]. Cellulose copolymerized with polymers such as poly(methacrylic acid) is used as a nanocarrier for photodynamic therapy agents, showing growth inhibition and selective tumor accumulation [49].

1.3.1.5 Crosslinking strategies of cellulose and its derivatives

To enhance mechanical strength, porosity, and stability, crosslinking of cellulose and its derivatives was used. For example, cellulose nanocrystals crosslinked with glutaraldehyde, which enhanced thermal stability and pore size, were used for releasing phycocyanin [50]. Carboxymethyl cellulose (CMC) crosslinked via biorthogonal inverse electron demand Diels-Alder (IEDDA) showed a high loading of DOXO and rapid release triggered by glutathione [51]. Dialdehyde CMC crosslinked with gelatin, then modified with folic acid, provides a pH-controlled anticancer drug delivery system, enhancing its efficiency in addition to bioimaging capabilities [52].

1.3.2 Cellulose as a drug delivery system

Drug delivery systems (DDS) are the formulations or technologies designed to control when, where, and how a drug is released in the body [53]. Conventional drug formulations, such as capsules, tablets, ointments, and syrups, have several limitations that affect therapeutic efficacy due to poor bioavailability, limited permeation, low solubility, and early drug degradation, especially for complex molecules like anticancer agents [54, 55]. So, there was a need for an advanced and smart DDS to overcome the limitations of conventional methods. Smart DDS, including Stimuli-responsive technologies that enable controlled, precise, and site-specific drug release responding to triggers like Temperature, pH, or enzymes, lowering toxicity and developing therapeutic efficacy [56].

Cellulose and its derivatives have demonstrated multifaceted, biocompatible, and sustainable properties as DDS materials, offering unique advantages such as high drug-loading capacity, tunable release profiles, and compatibility with numerous therapeutic agents. Recent research focused on the use of cellulose in various forms, including hydrogels, nanoparticles, beads, aerogels, and composites for oral, ocular, transdermal, and targeted cancer therapies [57-61]. The ease of chemical modifications and fabrication techniques has further expanded the functional landscape of cellulose-based DDS, enabling patient-specific and smart drug delivery platforms [62-64].

1.3.2.1 Modified cellulose in nanotechnology DDS

For the same reasons, we use cellulose; the cellulose nano-materials are used, although due to the unique properties of materials at the nanoscale, such as high surface area, target selectivity, and stability, which improve performance in many fields [65]. In medicine, nanotechnology enhances drug delivery by allowing precise targeting, increased bioavailability, and controlled release, which increases the efficacy and reduces side effects [66].

1.3.2.2 Types of cellulose nanocarriers

Mainly, nanocelluloses exist in the forms of nanofibrils (CNFs), cellulose nanocrystals (CNCs), and bacterial nanocelluloses (BNCs), each with distinct crystallinity, aspect ratio, and flexibility [67]. Carboxymethylation, phosphorylation, sulfation, mucoadhesion, enzyme responsiveness, and targeting ligand conjugation are possible modifications on nanocelluloses explored for DDS [67]. These modified nanocelluloses are used for controlled and extended release, enhanced solubility of drugs that are poorly soluble, and anti-inflammatory and anti-microbial effects

1.3.2.3 Smart cellulose-based drug delivery systems

Cellulose and its derivatives are used to make stimuli-responsive systems that release drugs in response to specific triggers, internal or external, to improve targeting and reduce side effects [68].

1.3.2.4 pH-responsive cellulose systems

Depending on the difference in pH value between the targeted tissues and healthy tissues, this smart DDS works. Thennakoon M. *et al*. showed that cellulose derivatives with ionizable groups swell or shrink with pH changes, thereby altering drug diffusion and porosity [68]. This type of DDS utilizes protonation/deprotonation of functional groups such as carboxyl and amine groups, or cleavage of pH-labile bonds, to alter porosity, swelling, or drug bonding, thereby achieving site-specific release [69, 70].

1.3.2.5 Temperature-Responsive systems

Using cellulose and its derivatives for drug release, depending on the temperature difference. Liu, Zhongming *et al.* combined carboxymethyl cellulose with polymer network aerogels and poly(N-isopropyl acrylamide) (PNIPAM) and showed efficient loading and sustained release of anticancer drugs due to dual temperature/pH responsiveness, allowing drugs such as 5-fluorouracil to be slowly released [71].

1.3.2.6 Ionic-Strength-Responsive systems

A promising application in cancer treatment has been demonstrated using ionic-strength-responsive systems, particularly in targeted drug delivery and controlled release, utilizing cellulose derivatives. Using Cellulose nanoadsorbents to capture chemotherapy drugs

under specific ionic conditions, to reduce systemic side effects without cytotoxicity [72]. Hydrogels composed of cellulose derivatives have been developed that change their physical state in response to ionic strength, enabling localized and sustained anticancer drug release, thereby reducing toxicity and improving therapeutic efficacy [73]. Nihat Gülçelik *et al.* have incorporated sulfonated reduced graphene oxide into a cellulose-based polyelectrolyte complex to enhance ionic strength sensitivity, conductivity, and mechanical strength [74].

1.3.2.7 Magnetic-Field-Responsive

By using a magnetic field to enhance drug delivery, targeted treatment, and tumor imaging. Iron oxide nanocubes are used to trigger ferroptosis-like cell death by Fenton reaction, boosted with a magnetic field, to promote tumor suppression and immune activation [75]. Under alternating magnetic fields, Magnetostrictive-piezoelectric nanoparticles activate the generation of reactive oxygen species (ROS), which effectively kill tumors with high therapeutic efficacy and biosafety [76]. Di Li et al. used Magnetic nanorobots to actively target tumors to improve localized chemodynamic therapy by generating cytotoxic radicals through glucose consumption [77]. Jianmeng Zhu et al. combined magnetic nanomicelles with pH sensitivity and magnetothermal effects to enhance tumor targeting and drug release [78].

Across these triggers, cellulose hydrogels are key because of:

1. Their 3D porous structure
2. Tunable degradation
3. Ability to encapsulate
4. Protect therapeutics

1.4 Cysteine

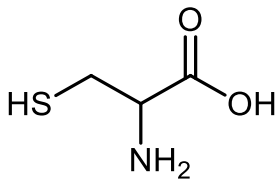

An amino acid containing sulfur; its IUPAC name is 2-Amino-3-sulfanylpropanoic acid, and it forms white crystals or a powder. The thiol groups confer it with an unusual reactivity in chemistry, biology, and drug design.

1.4.1 Chemical properties of cysteine

$C_3H_7NO_2S$, the chemical structure of cysteine:

- The thiol group can be ionized to form thiolates (S-) with a relatively low pKa, making cysteine one of the most redox-active and nucleophilic amino acids [79].
- Forms cystine, which is a derivative of cysteine formed by a disulfide bond, and helps in stabilizing proteins.
- Cysteine coordinates with metal ions in enzymes in the catalytic or regulatory sites.

1.4.2 Biological and pharmaceutical roles

- Essential in preparing glutathione antioxidant, and helps in regulating redox homeostasis and signaling.
- a precursor for H2S, coenzyme A, taurine, and biotin.
- a source of energy and biomass, because of its carbon content.
- Its metabolism is reformed in cancer cells, which eventually serves as an anticancer strategy.

1.4.3 Uses of cysteine

In medicine, there is a specific form of cysteine called N-acetylcysteine (NAC) that is usually used in hospitals to treat paracetamol overdose and, sometimes, to clear lung receptors from mucus because it acts as a mucolytic and is studied for cardiovascular disease. And showed a good metal chelation. And neurodegeneration, and nephroprotection as well.

1.5 Doxorubicin

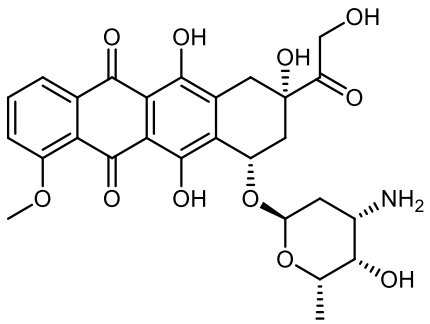

This compound is a significant chemotherapeutic agent with demonstrated efficacy against various cancer types, including hematological malignancies, breast cancer, and solid tumors. Its anticancer effects are primarily mediated through three mechanisms:

1. Intercalation into DNA.
2. Inhibition of topoisomerase II.
3. Induction of reactive oxygen species (ROS) generation.

These mechanisms lead to cell death [80]. However, its benefits are limited because it is dose-dependent and often irreversible toxicities, such as myelosuppression, and most notably cardiotoxicity, gonadotoxicity, and nephrotoxicity [81]. The therapeutic index of DOXO can be improved by a new technique, such as combination therapies and liposomal formulations, which has led to a reduction in toxicity and overcoming drug resistance [82].

1.5.1 DOXO chemical structure

DOXO anthracycline anticancer drug, and its chemical structure consists of a sugar moiety called denopamine linked to a planar anthraquinone aglycone. The DOXO molecule has two main functional groups, which help in conjugation. The first one is the primary hydroxyl group on the aliphatic ring chain [83]. The chemical structure participates in its action, where the planar ring intercalates into DNA; on the other hand, the amino group forms hydrogen bonds. The sugar moiety can be modified to reduce side effects like cardiotoxicity and enhance anticancer activity [84]. In order to identify reactive sites and electronic properties, quantum mechanical studies have been done that inform drug design.

1.5.2 DNA intercalation

The anticancer efficacy of DOXO comes primarily from the DNA intercalation, by inserting itself in between base pairs in nucleosome-free regions of chromatin, which disrupts critical cellular processes, including histone eviction, also leads to DNA damage, inhibition or trapping of topoisomerase II, which is an enzyme responsible for DNA replication and repair, and transcription arrest by degrading RNA polymerase II [85]. The combination of these effects leads to changes in DNA, including the formation of alternative DNA conformations that effectively trigger apoptosis.

1.5.3 DNA-binding mechanisms of DOX

One of the major mechanisms of DOXO is dependent on the binding to the DNA through interposition between base pairs, adding to it hydrogen bonds, and groove binding, especially at the N7 site of adenine, involving a two-step mechanism, a rapid groove binding to segments of DNA with a high concentration of adenine (A) and thymine (T), called AT-rich regions, which is important region for DNA replication initiation, because of the weak bond between A and T allows easier unwinding, and then a slower intercalation follows the fast binding, but into guanine and cytosine rich regions, which forms a high affinity and stable complexes [86]. The major driving force for a stable DOX-DNA complex is van der Waals interactions, as revealed by molecular dynamics simulations and free energy calculations, whereas solvent and electrostatic effects can resist binding. Torsional stress, a DNA structural feature, facilitates the drug's intercalation, with nucleosomal DNA showing impulsive intercalation more than linear duplex DNA [87].

1.5.4 Enhancing the safety of DOXO

Due to the adverse effects and toxicity of DOXO, various strategies were used to overcome its limitations, which we mentioned earlier, focusing on multiple approaches such as combination therapies, novel formulations, and molecular targeting. Nanoformulations and liposomes improve drug delivery, reduce cardiotoxicity, and aid in bypassing resistance mechanisms by enhancing tumor targeting [88]. Natural compounds like curcumin, cannabidiol, and flavonoids such as apigenin, chrysin, and luteolin, when combined with DOXO as Combination treatments, showed promise in reducing toxicity and reversing resistance by modifying oxidative stress and drug efflux

pathways [89]. Molecular pathways can be targeted with Nuclear Factor Erythroid 2-Related Factor 2 (Nrf2), which is involved in drug resistance and the oxidative stress response, providing a dual benefit of protecting normal cells while exposing cancer cells to doxorubicin [90]. Additionally, K. Chegaev et al. made novel derivatives such as H_2S-donating doxorubicin compounds, which demonstrate activity against resistant tumor cells and reduced cardiotoxicity [91]. Others used prokineticin-2 as a biomarker to predict and overcome resistance [92].

1.5.5 Challenges of delivering doxorubicin

Delivering DOXO faces various challenges, such as systemic toxicity, multidrug resistance in tumors, and dose-limiting cardiotoxicity. But nanocarriers, including liposomes, metal-organic frameworks, micelles, and cyclodextrin-based nanoparticles, have been developed to improve tumor targeting and control drug release; however, issues such as premature drug leakage, uneven drug loading, immunogenicity, and limited circulation time remain significant challenges [93]. M. Mahani et al. used modified carbon quantum dots, and N. Akhtar et al. used superparamagnetic iron oxide nanoparticles to increase the cellular consumption and site-specific accumulation, but the challenges are still there in reaching sufficient tumor entry [94, 95]. Nanocarriers that release DOXO in response to redox, pH changes, or light show good results in lowering cardiotoxicity and enhancing intracellular delivery. But still clinically limited [96].

1.5.6 Using Cellulose-based materials for DOXO delivery

Various benefits can be achieved by using modified cellulose as a DOXO delivery, including controlled release, enhanced drug loading, and improved biocompatibility. For example, the loading capacity of DOXO can be achieved by the modification of bacterial cellulose with alginate [97]. Nusheng Chen et al. used modified CMC and combined it with pH-sensitive micelles to form an injectable hydrogel that enables localized, continuous DOXO release and improves therapeutic control [98]. Additionally, the use of functionalized cellulose nanocrystals can achieve high drug loading via electrostatic interactions, leading to pH-triggered release and improving cellular uptake and anticancer efficacy by lowering systemic toxicity [99]. Combining cellulose derivatives with materials like ZnO nanoparticles to form a nanocomposite hydrogel, which optimizes DOXO delivery and cytotoxic effects [100].

1.6 Quercetin

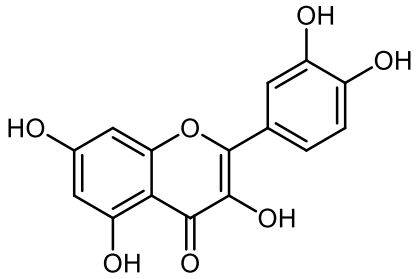

It is a natural flavonoid found mainly in fruits, grains, and vegetables, frequently present as glycosides like quercetin-3-O-glucoside, which is responsible for the pigmentation of many plants [101]. Its biological activities are varied, including anti-inflammatory, strong antioxidant, antimicrobial, antiviral, anticancer, and cardioprotective effects, making it effective in preventing chronic diseases such as cancer, diabetes, cardiovascular disease, and neurodegenerative disorders [102]. Its antioxidant activity comes mainly from the five hydroxyl groups that sweep reactive nitrogen and oxygen species, saving cells from oxidative damage. Even though the use of quercetin clinically is limited due to several causes, including low bioavailability, poor water solubility, and rapid metabolism, various delivery systems were developed to overcome these limitations, to improve solubility, stability, and absorption.

1.6.1 Chemical structure

Generally, it consists of two benzene rings linked by a heterocyclic ring; the two hydroxyl groups on the B ring primarily serve as redox/metal-chelating sites. The 3-OH with 4-oxo and C2=C3 double bond on the C ring is for extending conjugation and stabilizing radicals, and another two hydroxyl groups for additional H-bonding and chelation [103].

1.6.2 Quercetin anticancer mechanisms

Quercetin works in more than one way. Firstly, initiation of cell death can be done through different processes, including apoptosis, which is a natural process of programmed cell death that eradicates damaged and unneeded cells, to support health and prevent inflammation. Extrinsic death pathways are another process of induction of cell death, which enhances the tumor necrosis factor (TNF), increasing cell sensitivity to the TNF

superfamily. Then comes the Cell-cycle arrest, which inhibits cyclins and causes G1, S, or G2/M arrest depending on cell type [104].

Secondly, modification of cancer causes:

1. Blocking PI3K/Akt/mTOR, which is an intracellular signaling that controls the cellular functions, growth, proliferation, metabolism, and including survival, and. So, hibiting them in cancer cells will lead to reducing growth, survival, and glycolysis, and promoting autophagy [104].
2. Adjusting Mitogen-Activated Protein Kinase (MAPK) and its subfamilies to favor pro-apoptotic signaling [104].

Thirdly, oxidative stress, metastasis, and metabolism:

1. At pharmacologic doses, quercetin shifts from an antioxidant that reduces oxidative stress in normal cells to a pro-oxidant in cancer cells, increasing ROS levels and leading to the death of cancer stem cells [104].
2. Aims in mitochondria and glucose metabolism, reduces ATP, blocks glycolysis, and promotes apoptosis [105].

1.6.3 Solubility and stability of quercetin

Quercetin is a bright yellow, lipophilic, and practically water-insoluble powder, but soluble in lipids and alcohol.

1.6.4 Quercetin solubility in water

The direct measurements of the solubility of quercetin in water at 25 °C, 1-10 mg/L, which is a wide range according to the literature. [106]. The solubility of anhydrous quercetin in subcritical water increases from 0.00215 g. L^{-1} to 0.665 g. L^{-1}, but for quercetin dihydrate, from 0.00263 g. L^{-1} to 1.49. The wide range in solubility is because the solubility depends on a lot of factors, including polymorph, filtration, suspension time, and analytical method [106]. Glycosylation of quercetin increases cytosolic solubility and hydrophilicity [107].

1.6.5 Methods to improve solubility

1. Surfactants and micelles

   Using Tween 80 increases aqueous solubility, using micelles such as Pluronic P123 to encapsulate quercetin in a ~22nm hydrophobic core, and solubilization is achieved by hydrophobic interactions [108].

2. Protein and emulsions based on protein

   dispersions at the nanoscale formed from whey protein, caseinate, and soy protein solutions with quercetin (≈53–208 nm) [109].

3. Liposomes and Pickering

   Quercetin can be protected from oxidation and pH changes through liposomal encapsulation; 65-90% of quercetin has been preserved with proliposomes for more than 60 days at pH 7.4, compared to rapid loss in solution [106].

4. Solid dispersions

   Dispersion with Polyvinylpyrrolidone (PVP) or cellulose derivatives inhibits recrystallization and increases aqueous concentration. PVP amorphous solid dispersions show fast, complete release and are protected against degradation [110].

1.6.6 Quercetin chemical stability

Ilja Gasan Osojnik Črnivec et al. claim that the aqueous solution of quercetin with a pH range of 6-8 is stable for less than 4.5 hours at 4 °C in the dark, and the stability is best in the acidic environment, pH 2-4, and the stability decreases as the temperature increases and in light exposure [106]. In cell culture medium at 37 °C, quercetin is not stable and forms degradation products. It was noticed that ascorbic acid can improve the stability by increasing the antiproliferative effects and preventing auto-oxidation [111].

1.6.7 Quercetin DDS

Quercetin shows strong anticancer activity, but its poor solubility and bioavailability hold back its anticancer activity. Not forgetting that free quercetin is hydrophobic, unstable, and rapidly metabolized. And these reasons reduce the bioavailability and clinical impact. So the DDS was explored to avoid these obstacles, including enhancing the solubility, protecting from metabolism and degradation, and enabling controlled or targeted release.

DDS for quercetin used PVP K30 as a supersaturated drug delivery system (QSDDS) to keep quercetin in a supersaturated state for more than 12 hours, compared to quercetin suspension. QSDDS shows a 10-fold increase in oral bioavailability, a higher drug loading of 13%, and a simpler preparation for industrial-scale production [112].

Thanh Huyen Tran et al. improved solubility and intestinal absorption with self-nanoemulsifying drug delivery systems (Q-SNEDDS), to improve the quercetin level in plasma by 3-fold in rats [113].

1.7 Novelty and objectives

The selection of cellulose as a backbone for this delivery system is based on its abundance as a natural organic polymer, its exceptional biodegradability, and its high biocompatibility. Chemically, the presence of the primary hydroxyl group at C6 and the two secondary hydroxyl groups at C2 and C3 favored this selection. While cellulose nanocrystals offer a high surface area to volume ratio, the essential hydrophilicity along the CNCs makes them ineffective in the use of hydrophobic compounds or non-ionizable compounds. This study offers the modification of the surface of CNC and the functionalization of it with amine moieties to adjust its physicochemical properties. The innovation started with two parallel lines; the first one was the preparation of cellulose modified with cysteine, with two main steps:

1. Selective Tosylation: a reactive site for further modification was obtained by targeting the primary hydroxyl group on the C6 position and leaving the two secondary hydroxyl groups intact.
2. Amino Acid Functionalization: The tosylated cellulose prepared in the first step is reacted with L-Cysteine, and the cysteine is specifically selected for its thiol functional group and its amine group, which gives the desired DDS the necessary H-bonding sites.

Multiple hydrogen bonding: The suggested system functions through a host-guest framework. Cys-cellulose polymer acts as the host, and DOXO and Quercetin act as guests. The mechanical attraction and the release profile are ruled by specific molecular interactions.

The schematic interaction between Cys-cellulose polymer and the DOXO or the Quercetin is maintained by hydrogen bonds formed between the thiol and amine groups of the modified cellulose with cysteine and hydroxyl, carbonyl, and amine groups inherent to the DOXO and quercetin molecules.

Enhance stability: By using a cellulose-based framework to provide superior mechanical strength and stability, it is sustainable compared to the conventional injectable hydrogels, which is exposure to breakdown.

The second line in this project was the transition from stable amine carriers to a pH-responsive carrier consisting of a cellulose hydrazone matrix, while other methods aimed at the modification of the C6 hydroxyl group, this method lies on the oxidation of cellulose with sodium periodate $NaIO_4$, targeting C2-C3 adjacent hydroxyl groups to convert them eventually into a reactive dialdehyde, forming dialdehyde cellulose DAC, followed by a reaction with hydrazine derivative to form the hydrazone bond which is affected with pH changes, as it remains stable at normal cells pH 7.4, while hydrolysis rapidly in acidic environment such as tumor tissues where the pH vary from 5.5 to 6.4 depending on the type of tumor tissue. This method gives desired properties such as easy drug-carrier interaction: the cellulose hydrazone will act as the host for DOXO in aqueous media through multiple features:

1. pH-triggered release: acting like a switch for the liberation of DOXO, because of the hydrolysis of the hydrazone bond in an acidic medium.
2. Multiple hydrogen bonds: due to the hydroxyl and carbonyl groups on the modified cellulose, which interact with the amino and hydroxyl groups on the DOXO.

1.7.1 Objectives

The general objective of this work is to synthesize a cellulose-based polymer with an amino acid and dialdehyde cellulose modified with hydrazone derivatives to use them in controlled release technology for the antitumoral drug doxorubicin (DOXO).

1.7.1.1 Sub-objectives

For the first line:

1. Synthesis of tosylated cellulose.
2. Replace the tosyl group with an amino acid (Cysteine).
3. Drug loading and solvent optimization .
4. Release study in vitro: spectroscopic kinetic monitoring with UV-vis to quantify drug release rates over specific temporal intervals.

For the second line:

1. Oxidation of cellulose nanocrystals to form cellulose dialdehyde.
2. Preparing cellulose hydrazone.
3. Optimization of loading to maximize entrapment efficiency.
4. Release study monitored by UV-vis.
5. Biological Validation: checking the system's cytotoxic potency and IC50 values against chosen cancers cell lines.

Chapter Two

Experimental

2.1 Materials

2.1.1 Chemicals and reagents

The chemicals used in this work were purchased from Sigma-Aldrich (Jerusalem) and used as received. The chemicals included Microcrystalline cellulose, lithium chloride anhydrous (LiCl), methanol (MeOH), and nitrogen gas (purity 99.9%), N-dimethylacetamide anhydrous (DMAc), triethyl amine (Et_3N), 4-Toluenesulfonyl chloride, and acetone, sodium periodate $NaIO_4$, p-Phenylenediamine (PPD)

2.1.2 Instrumentation

The pH was measured using a typical Jenway model 35 pH meter. UV-Spectrophotometry (UV–Vis SHIMADZU UV-1800) was used for all spectral measurements. THE LAB TRON LLS-A12 centrifuge was used for separating the reaction products and for separating modified cellulose loaded with anticancer drugs. Characterization of each product we obtained was mainly done using FT-IR (Thermo Scientific Nicolet iS5 FT-IR) at An-Najah National University in Palestine. All NMR analyses were carried out using Bruker Avance, 500 spectrometers (Fällanden, Switzerland) at the Chemistry Department (University of Jordan, Amman, Jordan). Magnetic stirrer, rotary evaporator, freeze-drier

2.2 Methods

2.2.1 Synthesis of cellulose/DMAc/LiCl system

The preparation of cellulose tosylate (Ts-Cellulose) involves an extensive process to ensure that the water is completely removed. Starts with preparing a cellulose/DMAc/LiCl system. Cellulose activation started by soaking 5.0 grams of cellulose (0.03 mole of anhydrous glucose repeat unit) in 100 mL of distilled water in a 250 mL round-bottom flask. The soaked cellulose was stirred magnetically at room temperature for 2 hours. Then, the cellulose was collected by suction filtration. The collected cellulose was suspended in 100 mL of methanol for 1 hour. To ensure the water was totally removed, the cellulose was filtered by suction filtration. Then this step was

repeated twice to ensure the water was totally removed. The collected cellulose was suspended by stirring in 100.0 mL of N-dimethyl acetamide (DMAc) for 1 hour, then filtered, and this step was repeated twice. Then, the suspension was suspended in DMAc for three hours to remove the methanol, and then the cellulose was collected by filtration. In a clean, dry 250 mL round-bottom flask, 8 grams of LiCl was added to 92 mL of DMAc to prepare a 2.0 M LiCl solution, then stirred until the solution became clear. After this, the suspended cellulose, while it is still wet, was added to the LiCl solution and stirred until a clear gel was obtained.

2.2.2 Preparation of cellulose tosylate

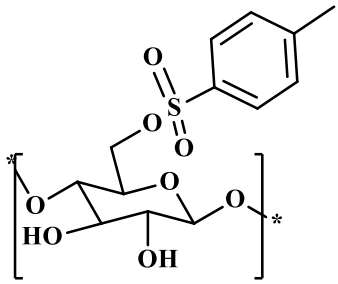

A 6.0 mL of dried triethylamine was added to the cellulose/DMAc/LiCl system, and then 18.0 grams (3:1 molar ratio) of p-toluene sulfonyl chloride was added to the solution, and the mixture was stirred at room temperature and under nitrogen overnight. After the reaction was completed, acetone was added dropwise under stirring as an antisolvent, then the precipitate was filtered, and the filtrate was washed with acetone.

2.2.2.1 Preparation of Cellulose-Cysteine

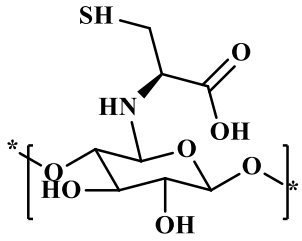

To prepare the modified cellulose with cysteine (Cell-Cys), an excess amount of L-Cysteine Hydrochloride monohydrate, 0.83 g (4.72 mmol), was added to 1.0 g of Ts-Cellulose (3.0 mmol), 1 to 1.5 molar ratio (Ts-Cellulose DS = 1: L-Cysteine hydrochloride monohydrate), in 20 mL DMAc and 0.5 mL Et_3N, stirred and refluxed for

3 hours at 80 °C. The reaction mixture was poured into methanol as an antisolvent, and the generated white solid was collected by filtration.

2.2.2.2 Preparation of Cellulose-Arginine

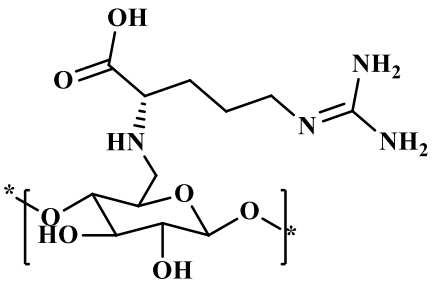

Starting with an excess amount of L-Arginine 1.1 g (6.0 mmol) dissolved in 10 mL of water, then adding to a tosylated cellulose suspension consisting of 1.0 g of tosylated cellulose (3 mmol) suspended in 10 mL of DMAc in a 50 mL round-bottom flask. A 0.5 mL of triethylamine was added to the reaction mixture as a base. Then the reaction mixture was refluxed for 3 hours under stirring at 80 °C. The DMAc solvent was evaporated by a rotary evaporator under vacuum to remove most of the solvent, and then the collected product was freeze-dried with a freeze-drier until dry, and caramel-colored flakes were collected. A solubility test was performed, and the product was soluble in methanol.

2.2.2.3 Preparation of Cellulose-Melamine (Cell-Mela)

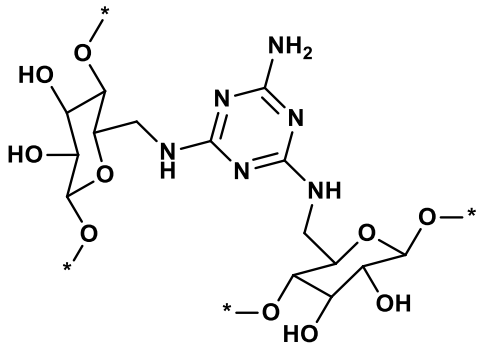

A 1.0 g (3.0 mmol) of Cell-TS and 1.1 g of melamine (10.0 mmol) were added to a mixture of 20 ml of DMAc and 20 ml of water as solvents in a round-bottom flask. The reaction was refluxed and stirred at 80 °C. Tetrahydrofuran (THF) was used as an antisolvent, and the resulting solid was filtered under suction. A white powder was collected. The product has the ability to swell in water due to crosslinking.

2.2.2.4 Preparation of Cellulose-p-phenylenediamine (Cell-PDA) and (Cell-PDA-Cell)

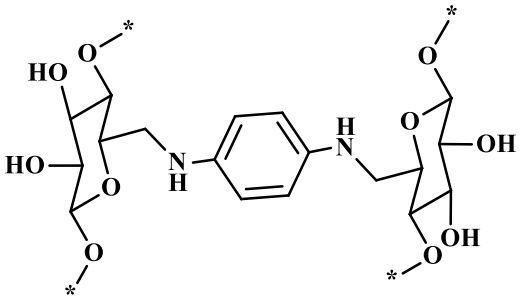

A 1.0 g of Ts-Cellulose (3 mmol) and 0.65 g (6 mmol) of p-phenylenediamine were added to a 15 ml THF in a round-bottom flask, and the reaction was heated at 40 ^{o}C with stirring for 3 hours. Acetone was added to initiate precipitation; the produced precipitate, which turned red to brown, was collected and washed with acetone several times. FT-IR was done to check if the product was formed. peaks at 3320 cm^{-1}, which is a good indication of the presence of N-H, while the two peaks at 1606 cm^{-1} correspond to the aromatic ring of the p-phenylenediamine. There appears to be a band around 1287 cm^{-1}, which is typical for Aromatic C–N stretching, and the 628 peak corresponds to the N-H bending. The most important thing is the disappearance of the S=O asymmetric stretching, proving that most of the tosyl groups are substituted with the amine group.

Depending on the nucleophilic substitution reaction for the tosyl group with the amine groups on the p-phenylenediamine to form a crosslinking between two cellulose chains, seeking to achieve a cuvette along the bulk polymer to encapsulate the anticancer drug in it, and if it didn't go for a cross-linkage, there will be a free primary amine to help capture the anticancer drug (DOXO) with hydrogen bonds.

2.2.3 Preparation of Dialdehyde Cellulose (Cell-A)

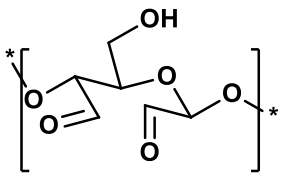

The preparation started with 10.0 g of microcrystalline cellulose suspended in 300 mL of distilled water, then 15.0 g of sodium metaperiodate $NaIO_4$ was added to the cellulose suspension in a 1.0 L beaker wrapped with aluminum foil (to prevent light from oxidizing

the cellulose), then stirred and heated for 3 hours at 40 °C. The mixture was filtered by suction filtration, and the white solid slowly turned yellowish in color after it dried.

2.2.3.1 Preparation of cellulose hydrazone

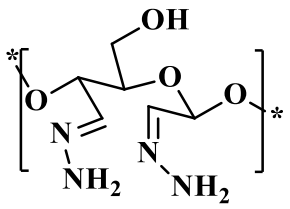

The reaction is a standard Schiff-base–type condensation between the aldehydes on C2 and C3 of Cell-A, and the –NH–NH2 group was preformed to give the cellulose hydrazone. The reaction started with a 5.0 g sample of Cell-A (31 mmol) suspended in ethanol in a 100 mL round-bottom flask, and 4 g of Hydrazine Hydrate 50% (60.0 mmol) was added to the suspension, along with 1 mL of acetic acid. The reaction was refluxed for 3 hours at 60 °C. The product was filtered by suction filtration. A yellow powder was obtained.

2.2.3.2 Preparation of Cell-A-Cysteine

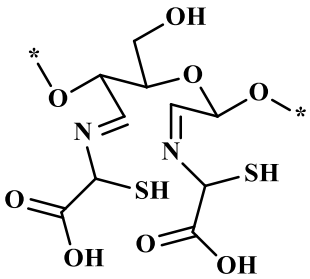

A 0.5 g (3.0 mmol) sample of Cell-A was added to 1.0 g of cysteine Hydrochloride monohydrate (6 mmol) suspended in 10 mL of DMAc in a 50 mL round-bottom flask, along with 1.0 mL of Et_3N as a base. The reaction was stirred and refluxed for 3 hours. A pale-yellow powder was obtained after filtration. The powder was allowed to dry. The resulting product was soluble in water.

2.2.4 Chemical inclusion of Doxorubicin (DOXO) in Cellulose Hydrazone (cell-HD)

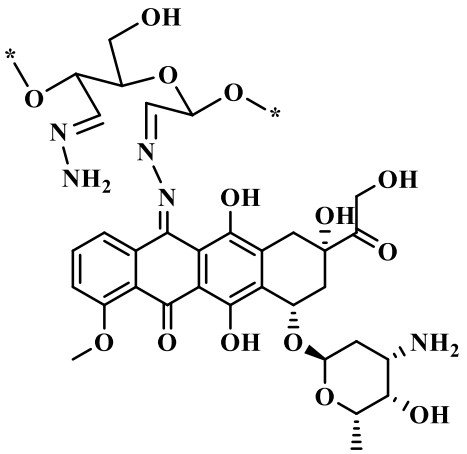

A mixture of 0.5 g cellulose hydrazone and 20 mg DOXO in 10 mL ethanol and 0.5 mL glacial acetic acid is heated under reflux for 24 hours. The reddish color of the reaction mixture became darker. Acetone was used to initiate solid precipitation; the red precipitate was collected by suction filtration. FT-IR was done on it. This product was tested for release study under different pH levels of 6.4 and 7.4.

2.3 Loading anticancer drugs on the modified polymers

2.3.1 Loading quercetin on Cell- Cys

A 10.0 mg of Cellulose-Cys and 11.0 mg of Quercetin dissolved in 5 mL of DMSO were dissolved in 10 mL of DMSO and stirred and sonicated, then 20 mL of 1% PEG (PEG in DMSO) was added dropwise under 510 rpm stirring. After centrifuging, the decantation of the solvent, 40 mL of water was added to dissolve the particles completely. The loading percentage was calculated using equation 1 by measuring the absorbance of the stock solution and the supernatant using a UV-VIS instrument at 378.5 nm.

Equation 1: percentage of loading efficiency of quercetin on Cell-Cys

$$Loading\ Efficiency\ (\%) = \frac{Abs.Querc.added - \text{Abs.}Querc.remained}{Abs.Querc.added} \times\ 100\%$$

2.3.1.1 Quercetin release study

The polymer (Cell-Cys) loaded with quercetin was examined for quercetin release at pH 6.4 and 7.4 in phosphate buffer, simulating the pH of normal cells and tumor cells, respectively. By inserting 2.0 mL of the Cell-Cys loaded with quercetin in a dialysis membrane in 5 mL of each phosphate buffer (7.4,6.4), 1 mL samples were taken at different intervals, and each 1 mL taken was replaced with 1 mL of the phosphate buffer. The quercetin concentration of each sample was measured using a UV-VIS instrument at 378.5 nm.

2.3.2 Loading DOXO on modified polymers

A 1.0 mL of DOXO solution (0.25 mg/ml water) was added to 0.5 g of each polymer (Cell-Cys, Cell-Hydrazone, and Cell-A) and allowed to dry at room temperature.

2.3.2.1 DOXO Release study

The release study was done on each loaded polymer with DOXO, which was tested for releasing DOXO at different pH levels, 6.4 and 7.4, in phosphate buffer, to simulate the pH of normal cells (7.4) and the pH of tumor cells (6.4).

2.3.2.1.1 Release study of DOXO loaded on Cell-A

A 30 mL of release medium was added to the 0.5 g loaded polymer, stirred at the magnetic stirrer at 50 rpm. A 1 mL sample was taken at different intervals (1,2,3,4,24,48) hours, and the samples' absorbance was measured with a UV-VIS instrument at 486.2 nm. This process was done at the two levels of pH 7.4 and 6.4.

2.3.2.1.2 Release study of DOXO loaded on Cell-Hydrazone

A 25 mL of release medium was added to the 0.5 g loaded polymer, stirred at the magnetic stirrer at 50 rpm. A 1 mL sample was taken at different intervals (1, 2, 3, 4, 24, 48) hours, and the samples' absorbance was measured with a UV-Vis instrument at 486.2 nm to obtain the cumulative amount released. This process was done at the two levels of pH 7.4 and 6.4.

2.4 Cytotoxicity

The cytotoxicity of the loaded DOXO Cell-HD and Cell-A was tested against HepG2, HeLa, LX-2, and MCF-7.

Polycarbonate plates were used in the cytotoxicity test, filled with culture growth medium (CGM), which was used to cultivate the cancer cells. that is made of DMEM medium augmented with 10% (FBS), L-glutamine, and pen/strep. The plates were kept in a humidified atmosphere with 5% CO_2 at 37 °C, in order to enhance cell proliferation.

Following confluency, cells went through two cycles of washing using 15 mL of calcium-free phosphate-buffered saline (PBS). 1 mL of trypsin was used to treat the cells, and then the plates were incubated for 3 min. To inactivate the trypsin. 10 mL of CGM was added to the plate. The cell suspension was diluted. The diluted cell solution was used to fill each well of a 96-well plate, then left to adhere in an incubator at 37 °C for 24 hours. 100 µl/well of each DOXO released from CELL-A-DOXO and Cellulose-hydrazone-DOXO, and pure DOXO was added to the plate, which was left to incubate for 24 hours. With a concentration range of 0.02 µg/ml to 80 µg/ml. 20 µL of MTS solution was added to each well, then left in the incubator for 2 h. The absorbance of each well was determined with a plate reader.

Chapter Three

Results and Discussion

The main objective of this work is to develop a natural-based polymeric material for the slow release of various cancer drugs. Several polymers with various functional groups were synthesized.

3.1 Preparation of cellulose cysteine (Cell-Cys)

The polymer was prepared as shown in Figure 5. The first step involved the synthesis of cellulose tosylate. In the first step, cellulose was dissolved in 8% LiCl/DMAc, then converted to the cellulose tosylate ester by reacting it with p-toluene sulfonyl chloride in the presence of triethylamine. In this reaction, a nucleophilic attack on the sulfonyl group displaces the chloride, which gets trapped by triethylamine as HCl. The second step involved reacting cysteine with Cell-Ts. Cysteine displaces the tosyl group by an S_N2 reaction to generate the first target polymer. The polymer was selected because it has several functional groups that make it suitable for making strong interactions with various cancer drugs, such as doxorubicin, via H-bonding and dipole-dipole. Cell-Ts and Cell-Cys were characterized using various spectroscopic techniques, including NMR (1H and 13C) and IR.

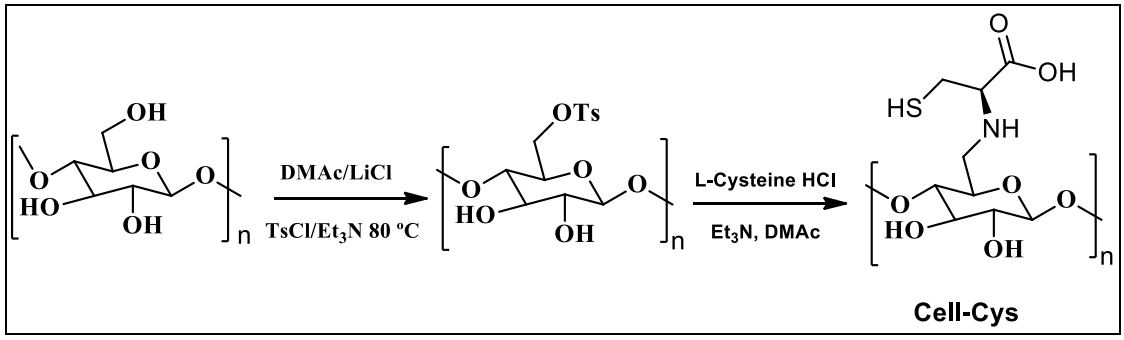

Figure 5: *Formation of cellulose tosylate ester and Cell-Cys.*

3.1.1 Characterization of cellulose tosylate

3.1.1.1 FT-IR of Cell-TS

Cell-Ts product was a white, soft, and semicrystalline material. The FT-IR spectrum of Cell-Ts is shown in Figure 7. It is compared with the IR spectrum of cellulose. The IR for pure cellulose obtained from Sigma-Aldrich in Figure 6 showed a peak at 3336 cm^{-1}

corresponding to the O–H stretching (broad), 2894 cm^{-1} for C–H stretching, the peak at 1428 cm^{-1} corresponding to CH_2 bending, 1163 cm^{-1} for C–O–C glycosidic, and 897 cm^{-1} for β-glycosidic linkage.

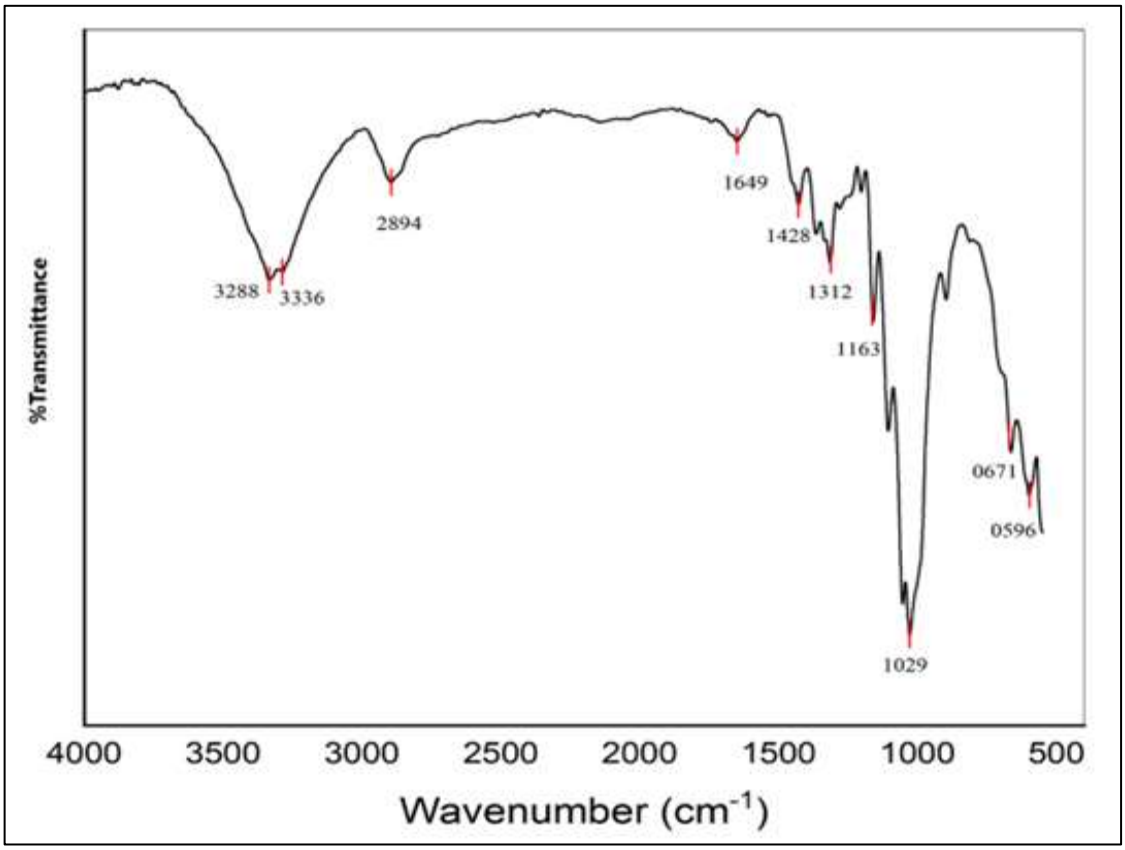

Figure 6: *IR spectrum of microcrystalline Cellulose.*

While the IR of cellulose tosylate we prepared shows a strong indication for the presence of the tosyl group, a peak at 1619 cm^{-1} for the aromatic ring C=C, 1396 cm^{-1} for SO_2 asymmetric stretch, 1171 cm^{-1} for SO_2 symmetric stretch, 1034 cm^{-1} for Ar–SO_2–O–C (sulfonate ester).

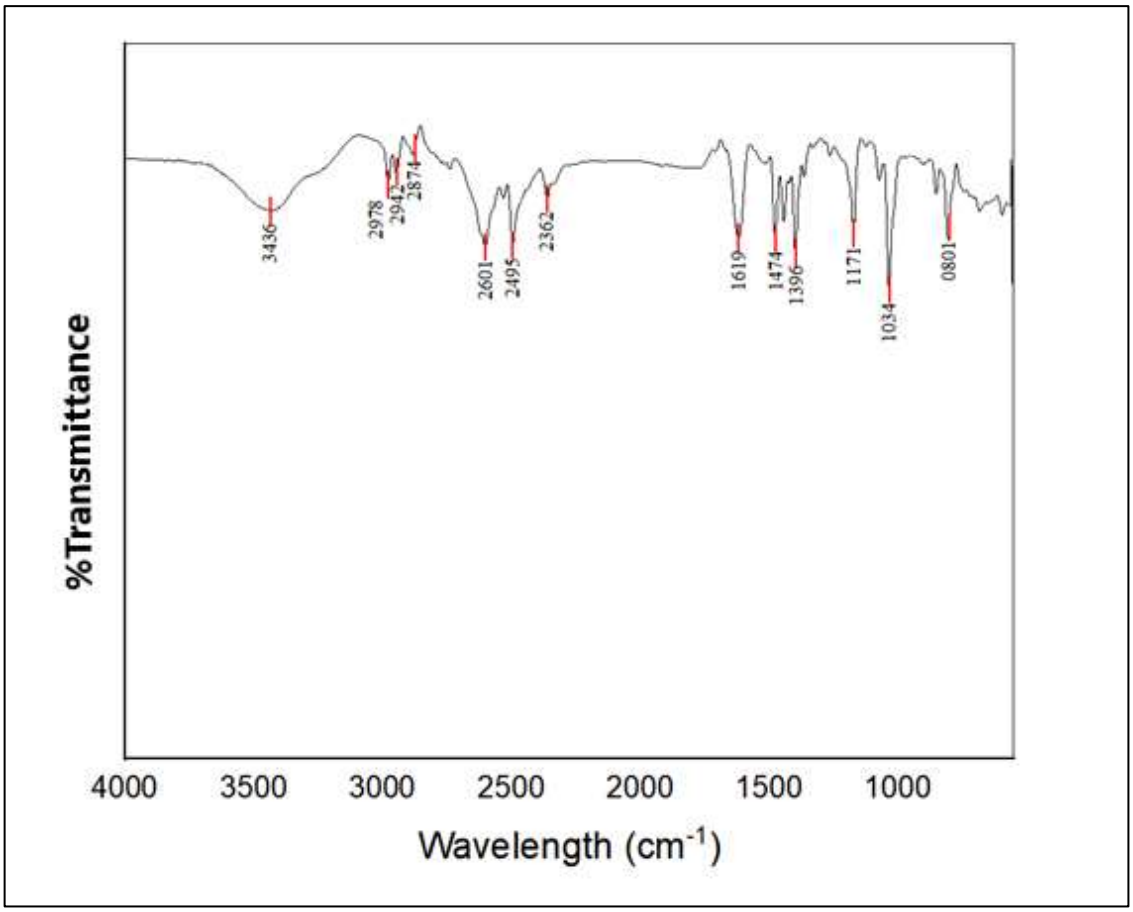

Figure 7*: IR spectrum of cellulose tosylate.*

3.1.1.2 NMR of Cell-TS

The proton NMR of Cell-Ts is shown in Figure 8. The spectrum reveals the correct structure, showing the aromatic protons at 6.8 ppm, the cellulose repeat-unit protons and the hydroxyl protons in the range 3.0 to 5.0 ppm, and the methyl on the benzene ring at 2.5 ppm. The results indicate that the degree of substitution is close to 2.0.

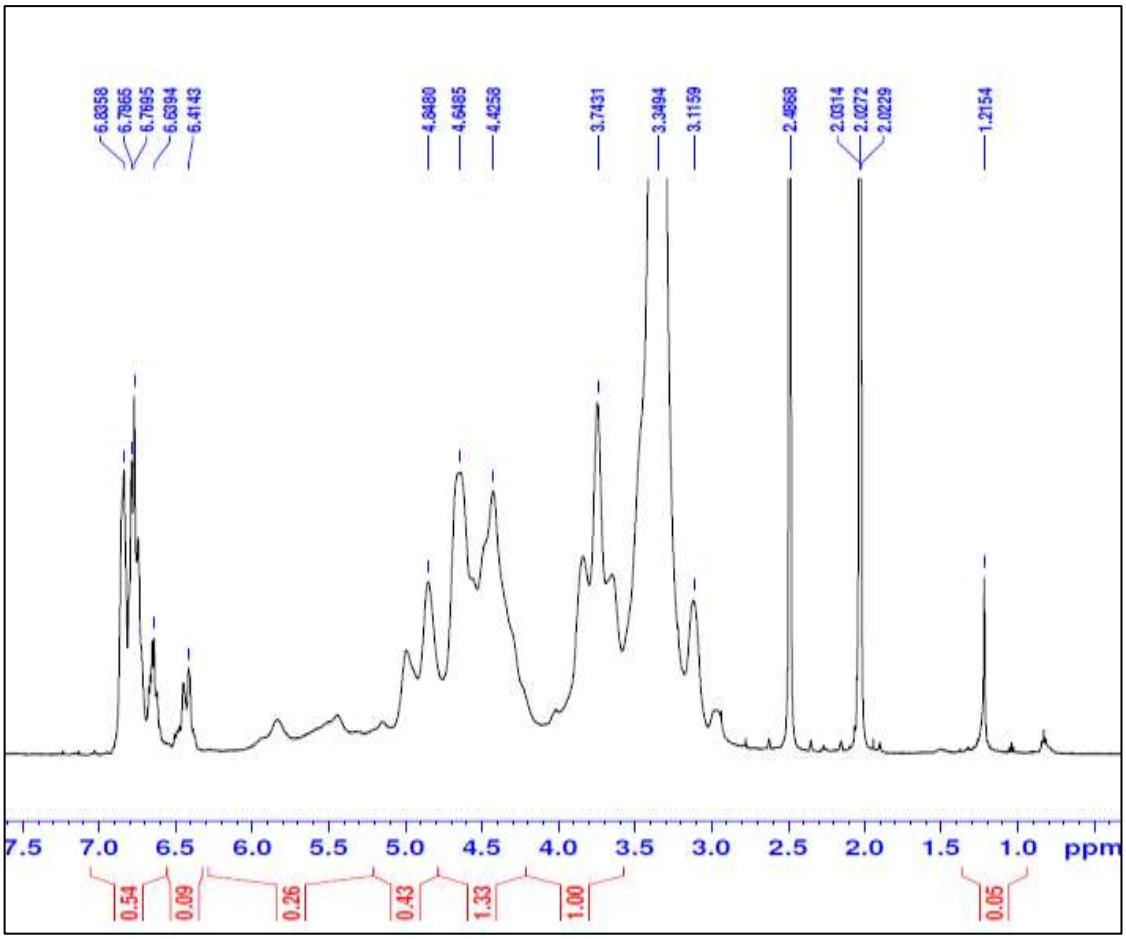

Figure 8: *proton NMR of Cell-Ts.*

3.1.2 Cell-Cys characterization and formation of nanoparticles

3.1.2.1 IR of Cell-Cys

The obtained IR spectrum of Cell-Cys is shown in Figure 9, The spectrum indicates the disappearance of the tosyl aromatic peak that clearly appeared in Figure 7, in addition to the disappearance of sulfonyl bands, together with the appearance of carboxylate stretching bands, COO- at 1579 cm^{-1} for the asymmetric stretch, and 1389 cm^{-1} for the symmetric stretch, and the appearance of thiol -SH band at 2540 cm^{-1}, which confirms the nucleophilic substitution of the tosyl group by cysteine through the amino functionality, producing N-alkylated cysteine-modified cellulose.

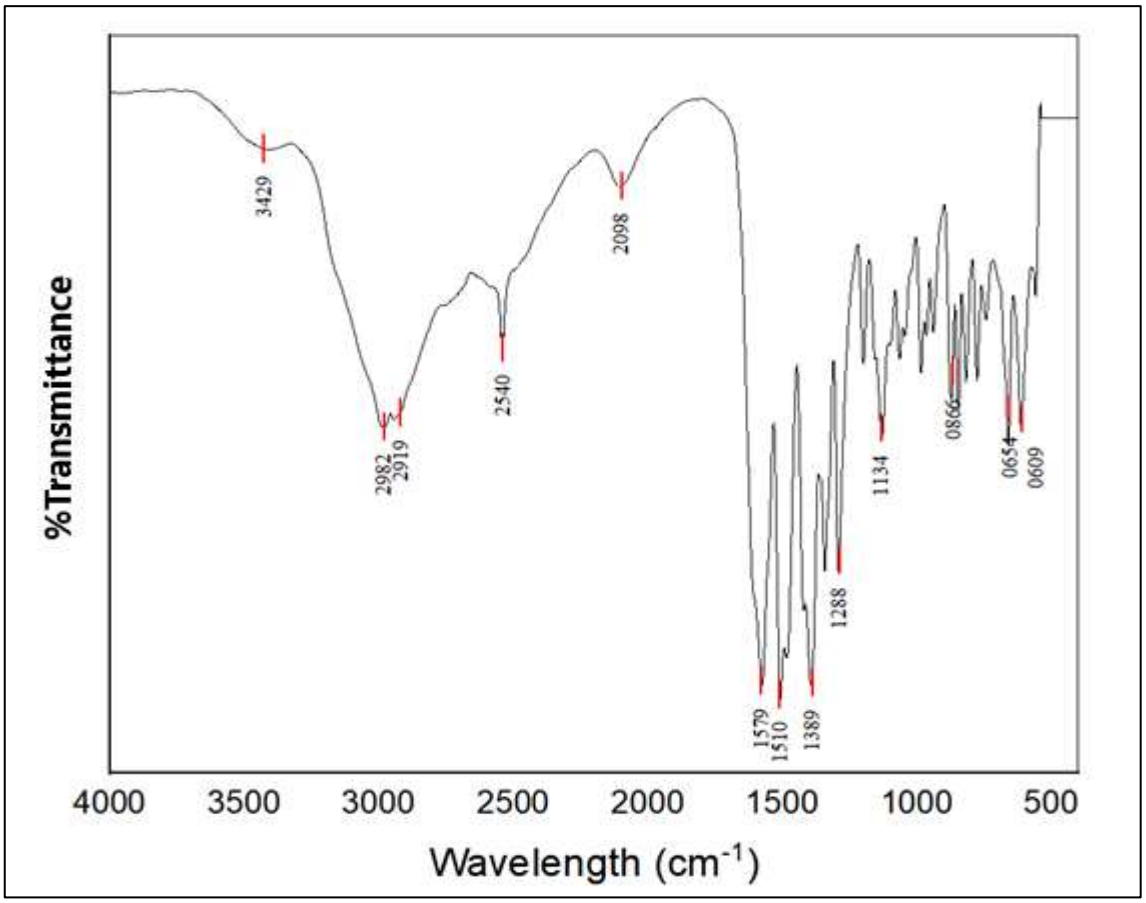

Figure 9*: IR spectrum for Cell-Cys*.

3.1.2.2 Cell-Cys nanoparticles characterization

The nanoparticles were made by dissolution of Cell-Cys along with quercetin or doxorubicin in DMSO, followed by slow precipitation with the dropwise addition of water under fast stirring, as shown in the experimental part (experimental section)

The produced particles were subjected to analysis by Dynamic Light Scattering (DLS)**.** It is an analytical technique used to measure the size of the particles, especially in the nanometer range, by illuminating the particles with a laser and screening fluctuations in scattered light.

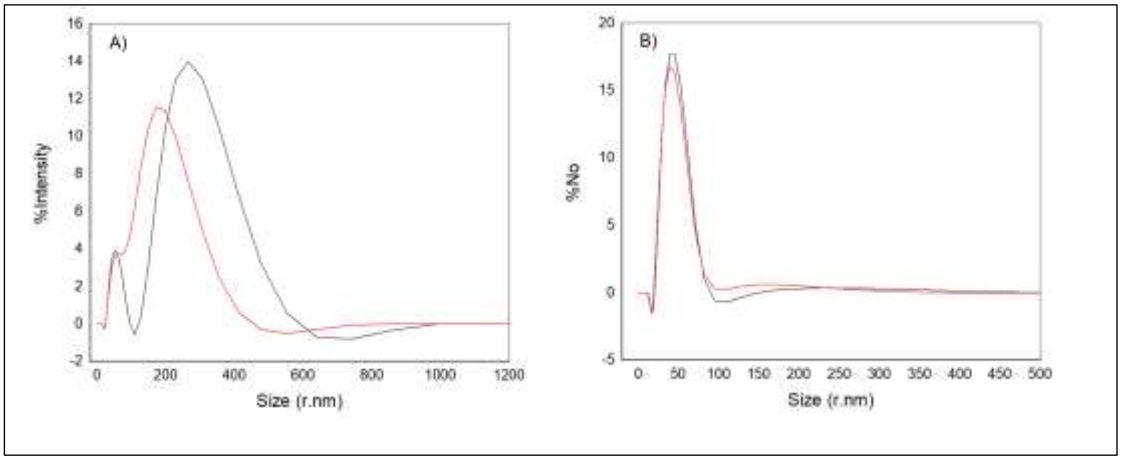

Figure 10*: Cell-Cys nanoparticles characterization.* A) Size Vs. %Intensity B) Size Vs. %Number for Cell-Cys Nanoparticles loaded with quercetin.

From the charts in Figure 10, the number-based size distribution shows that most of the particles have a radius between 35 and 45 nm, which is in diameter corresponds to 70 – 90 nm. On the other hand, the intensity distribution showed a larger apparent particle size due to minor aggregates, which scatter more light, reflecting the dependence of the intensity on light scattering.

The particle was also subjected to a zeta potential test, an important test that assesses the stability of nanoparticles and their surface charge by dispersing the particles in a liquid and determining the electrical potential at the slipping plane surrounding the particles.

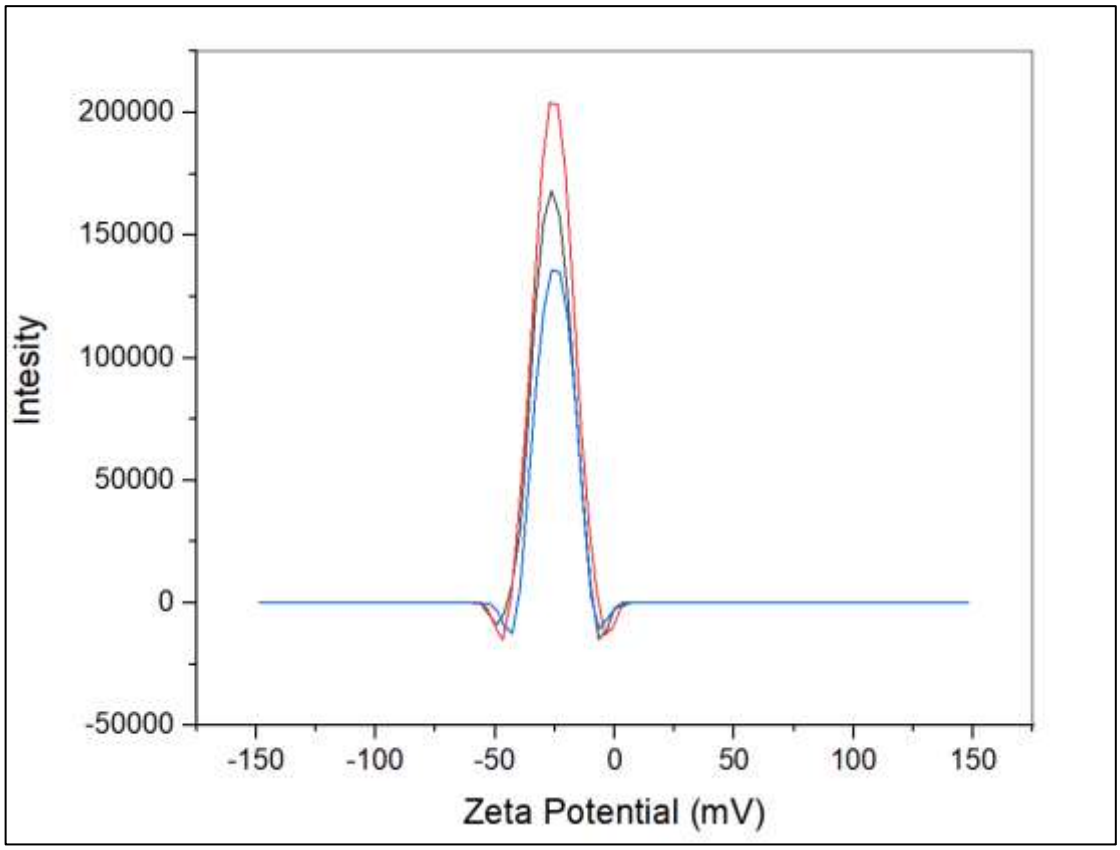

Figure 11*: Zeta potential for the Cell-Cys loaded with quercetin.*

The average of the zeta potential of the sample was around -28 mV, as shown in Figure 11. This value indicates a sufficient repulsive force between the particles, preventing the aggregation, leading to moderate to good electrostatic stability of the nanoparticle suspension. The negative value points to the ionization of functional groups present in the nanoparticles.

3.1.2.3 Loading of Cell-Cys nanoparticles with quercetin

After the loading of Cellulose-Cysteine with quercetin, the absorbance of the quercetin solution before the loading and the supernatant after the loading was measured using a UV-vis instrument at 378.5 nm, and the loading efficiency was calculated and found to be 17.04%.

3.1.2.4 pH-dependent release study of DOXO loaded on Cell-Cys

Depending on the properties of the cysteine moiety, at pH 7.4, the thiol group attached to the cysteine moiety remains protonated or forms stable interactions, establishing a thick network that traps DOXO. At pH 6.4, protonation could occur, which increases the release

of DOXO by different mechanisms: 1) increasing the hydrophilicity and swelling of the polymer, which opens up pores. 2) Disrupting H-bonding between the polymer and the drug. 3) changing the electrostatic repulsion/attraction.

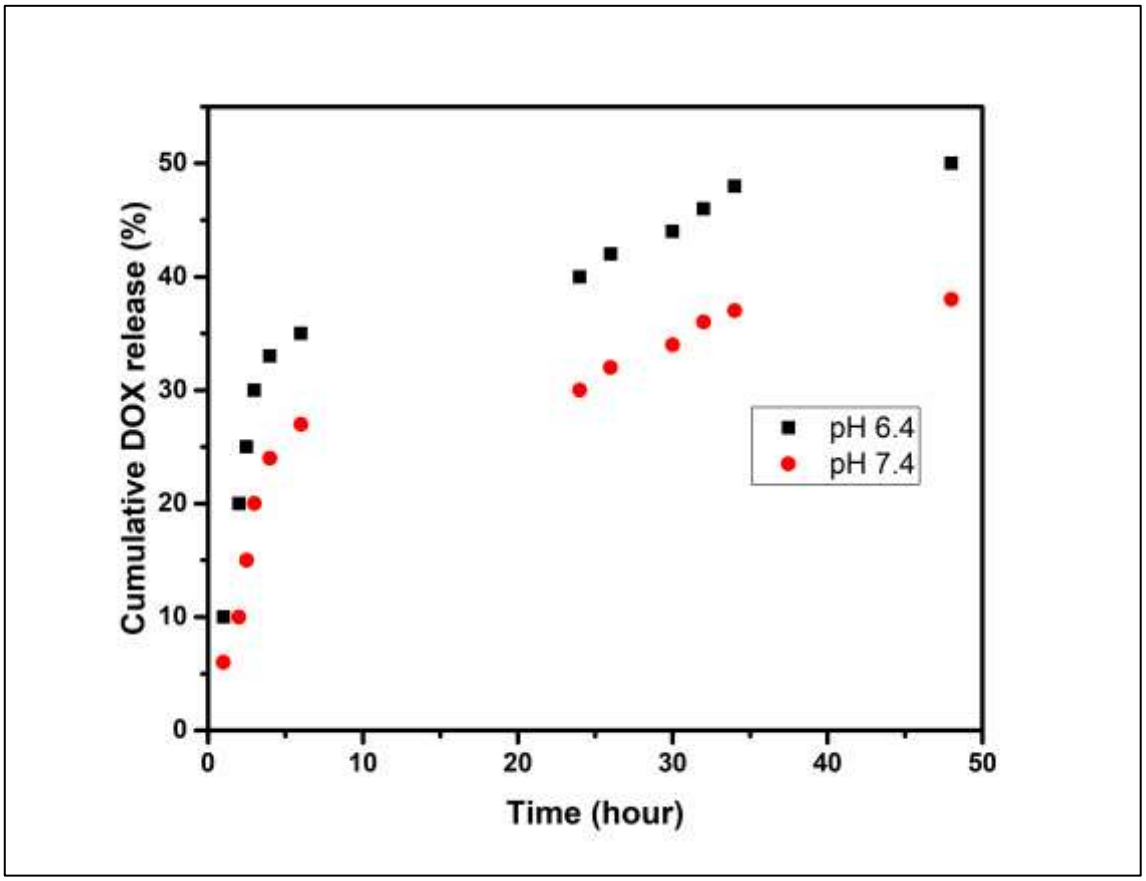

Figure 12: *Release of DOXO loaded on Cell-Cys at pH 7.4 and pH 6.4.*

From Figure 12, we observe significant pH-dependent release behavior. At pH 7.4, the release percentage was 20% at the first hour of the study, and increased gradually to reach 37.1% at the fifth hour of the study, while at pH 6.4, the release percentage was 20% at the first hour, and reached to 57.55% by the end of the fifth hour. This indicates the sensitivity of our system towards acidic conditions, which is highly desirable for cancer therapy, as it works as a pH-triggered DDS.

The amount released at pH 6.4 was 57.55% still leaves a portion of the drug in the system. A longer study time could be helpful to see if the system achieves complete release, as shown in Figure 12.

3.2 Preparation of Cellulose Melamine (Cell-Mela)

The preparation was performed by reacting Cell-Ts with an excess amount of melamine per anhydroglucose repeat unit. Melamine is a trifunctional amino compound; it is expected to act as a crosslinking agent by displacing the tosyl group through an S_N2 reaction. The product is expected to have a 3D structure with many amino groups distributed all over the structure, as shown in Figure 13. The amino groups may interact with doxorubicin via chemical and physical bonding. Chemical bonding could occur through the formation of an imine by reacting the amino group with the ketone of doxorubicin. This is unstable under acidic conditions of the human stomach. Physical bonding may occur through the formation of H-bonding between the polymer and the drug doxorubicin, as shown in Figure 13.

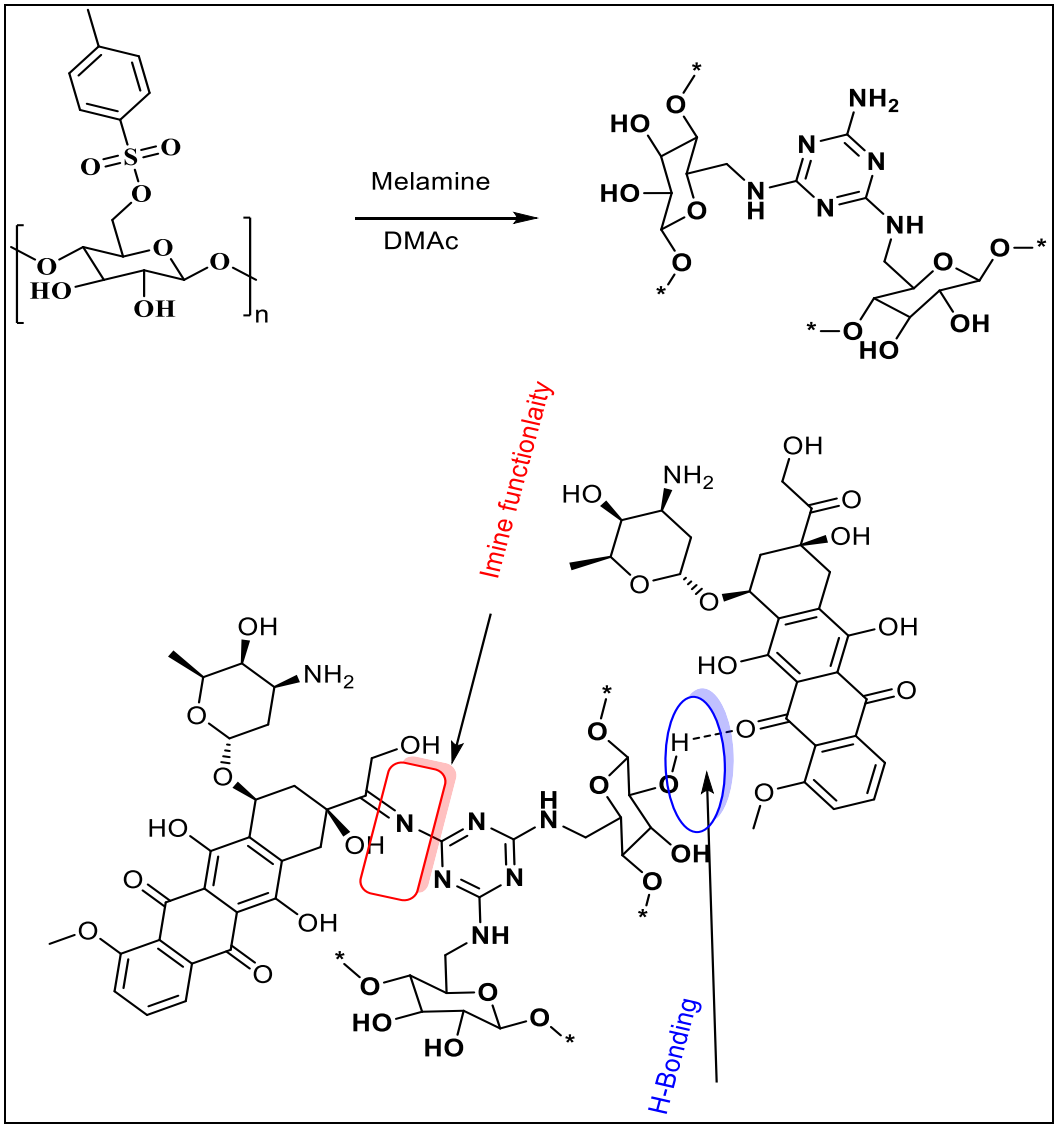

Figure 13: *Preparation of Cell-Mela and interaction with doxorubicin.*

3.2.1 Characterization of cellulose-melamine

3.2.1.1 Infrared Ft-IR

The IR spectrum of Cell-Mela is shown in Figure 14. The spectrum is expected to show a peak for a primary amine and a peak for secondary amine. In addition to a peak for triazene, and a disappearance of the sulfonyl peak bands. The IR spectrum in Figure 14 shows a strong indication of the substitution reaction, where the peak at 3512 cm^{-1} corresponds to N-H primary amine, while the peaks around 3389 cm^{-1} correspond to N-H secondary amine, and the peak at 1536 cm^{-1} is a strong indication of the presence of triazene stretching.

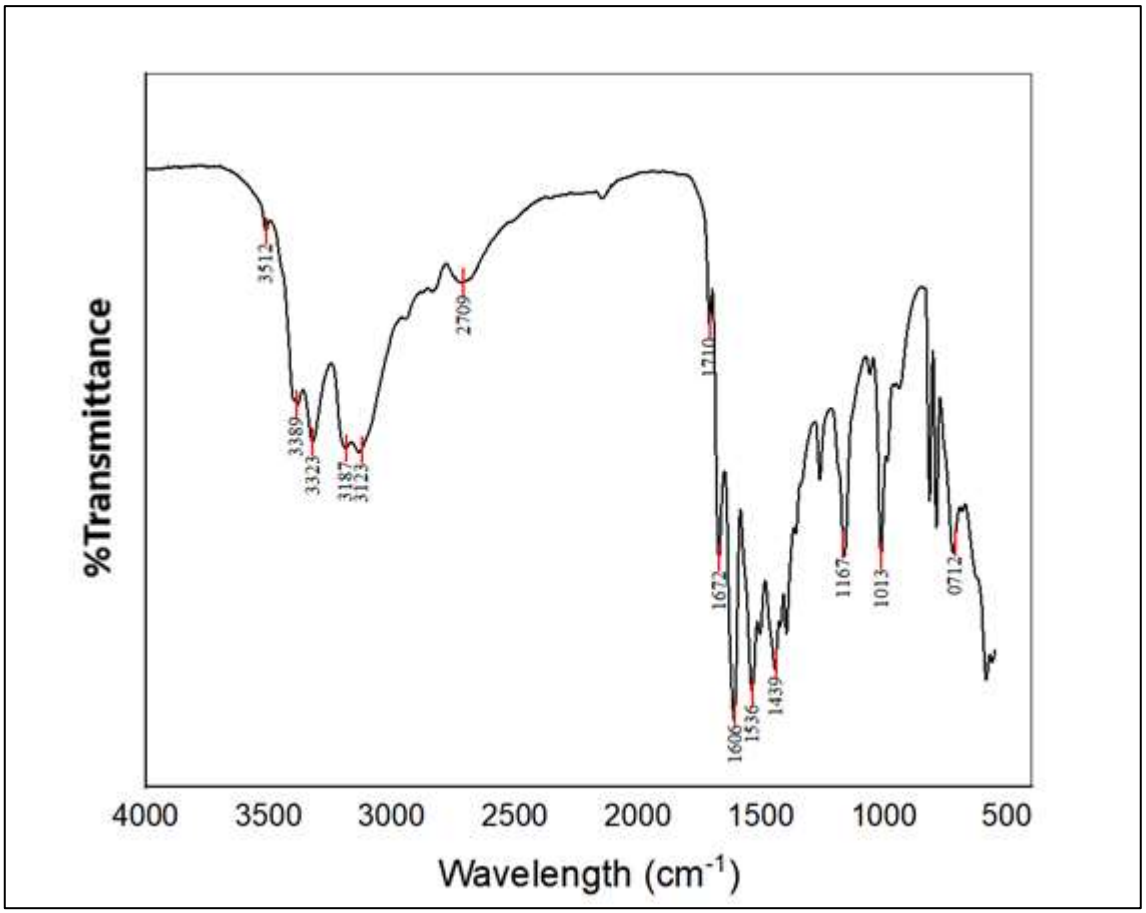

Figure 14: *IR spectrum for Cell-Mela.*

3.3 Preparation and characterization of Cellulose-p-phenylenediamine (Cell-PDA)

The preparation of Cell-PDA was performed using a similar process to that for Cell-Mela, by reacting Cell-Ts with an excess amount of p-phenylenediamine per anyhydroglucose repeat unit. p-Phenylenediamine is a difunctional amino compound; it is expected to act as a crosslinking agent by displacing the tosyl group through an S_N2 reaction. The product is expected to have a 2D sheet-like structure with many amino groups distributed throughout the sheet, as shown in Figure 15. The amino groups may interact with doxorubicin via physical interaction (H-bonding) as shown in Figure 15.

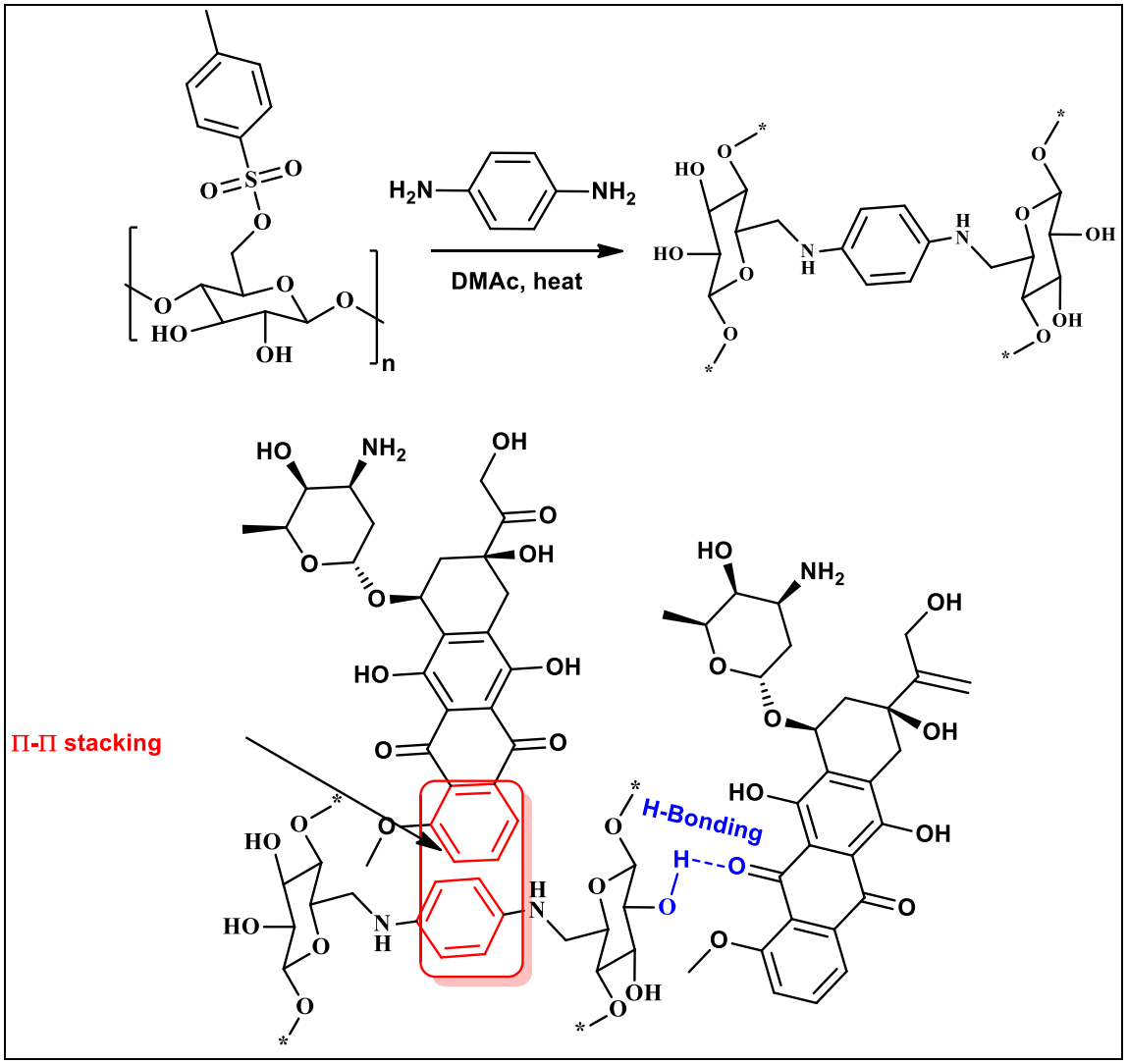

Figure 15: *Preparation of Cell-PDA and interaction with doxorubicin.*

The nucleophilic substitution reaction of the tosyl group with p-phenylenediamine primary amine is expected to show an indication for the replacement reaction by the disappearance of -SO_2- peaks and the appearance of -N-H secondary amine peak.

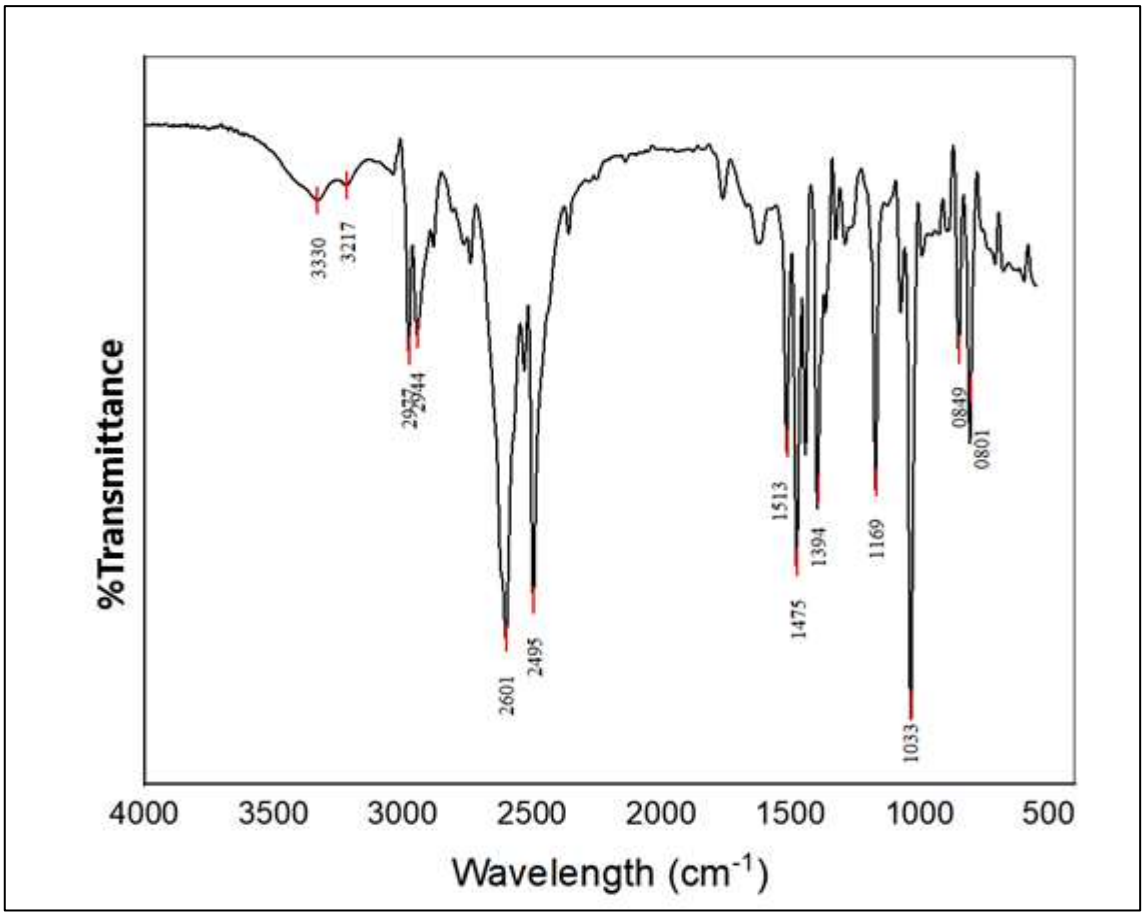

Figure 16: *IR spectrum of Cellulose-p-phenylenediamine.*

The IR spectrum shown in Figure 16 shows peaks at 3330 cm^{-1}, which is a good indication of the presence of N-H, while the two peaks at 1606 cm^{-1} correspond to the aromatic ring of the p-phenylenediamine. There appears to be a band around 1287 cm^{-1}, which is typical for Aromatic C–N stretching, and the 628 peak corresponds to the N-H bending. The most important thing is the disappearance of the S=O asymmetric stretching, proving that most of the tosyl groups are substituted with the amine group.

3.4 Preparation and characterization of Cell-A

The preparation was performed by oxidizing cellulose polymer with an excess amount of sodium periodate Figure 17. The reaction was carried out in water at 40 ºC. In this reaction, sodium periodate oxidizes the geminal hydroxyl groups to an aldehyde. The polymer was selected because it is amorphous, the polymer structure is accessible, and each repeat unit has two aldehyde groups that can react with the amino group of doxorubicin to form imine functionality Figure 17. The imine group tends to undergo hydrolysis in acidic conditions.

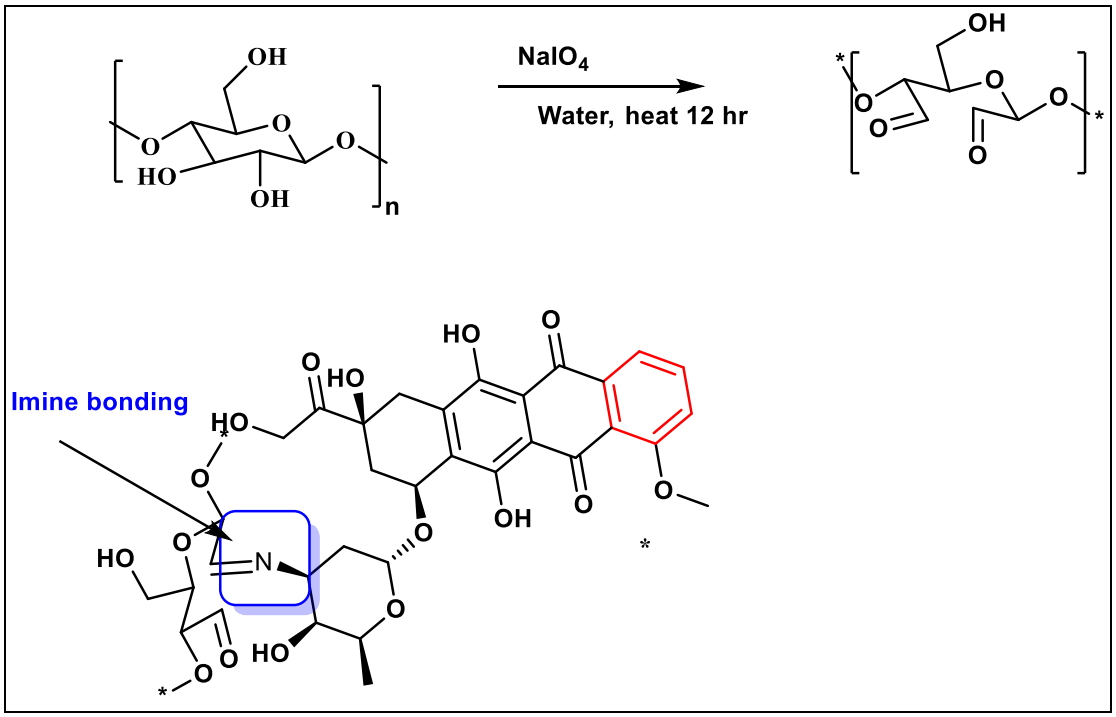

Figure 17: *Preparation of Cell-A and interaction with doxorubicin.*

3.4.1 Infrared spectrum of Cell-A

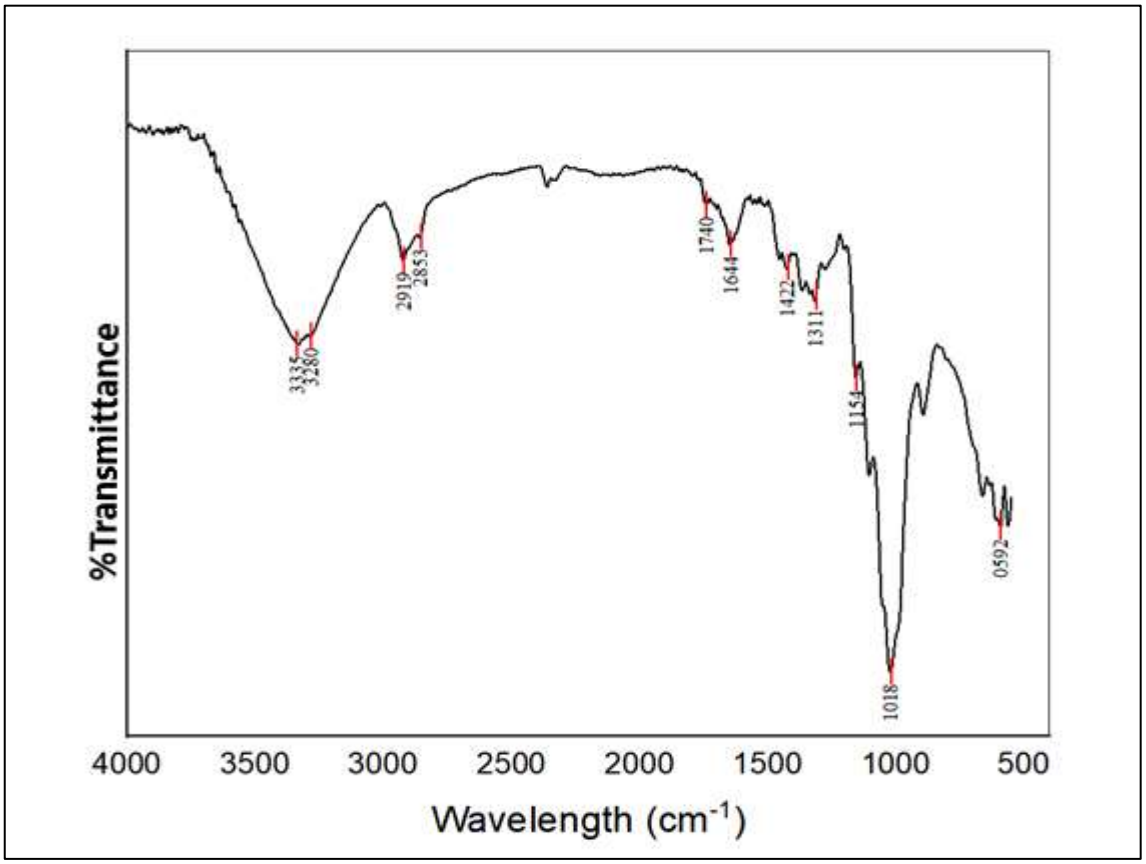

Figure 18: *IR structure of Cell-A.*

The IR spectrum of Cell-A is shown in Figure 18, it shows a strong and broad peak at 3335 cm^{-1}, indicating the presence of hydroxyl group stretching and strong hydrogen bonding, and the absence of the 1720–1740 cm^{-1} peak of the aldehyde carbonyl with the absence of the 2800-2700 cm^{-1} C-H of aldehyde group, caused by the instability of the dialdehyde cellulose, and the formation of hemiacetal between the aldehydes and the remaining hydroxyl groups on the cellulose, according to Lukáš Münster et al. as shown in Figure 19 [114]. The high number of -OH groups, which is responsible for the strong and broad peak at 3335 cm^{-1}.

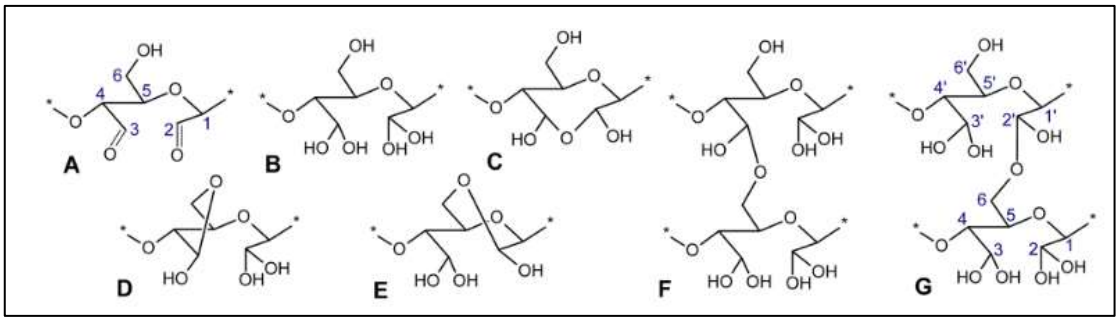

Figure 19: *Possible structures of Cell-A.*

3.4.2 pH-dependent release study of DOXO loaded on Cell-A

After loading DOXO into Cell-A, a release study was performed on the loaded modified polymer. The purpose was to evaluate the efficacy of the polymer in releasing the anticancer drug across different pH levels, simulating the pH of normal cells (7.4) and the pH of cancer cells (6.4). The principle of pH-responsive release depends on two factors:

1. Protonation of functional groups: at the acidic pH, the imine bond becomes protonated, leading to the release of the DOXO. At the same time, the electrostatic interactions between DOXO and the polymer weaken.
2. The increasing of the polymer swelling: the higher hydration of the polymer causes the expansion of the polymer network.

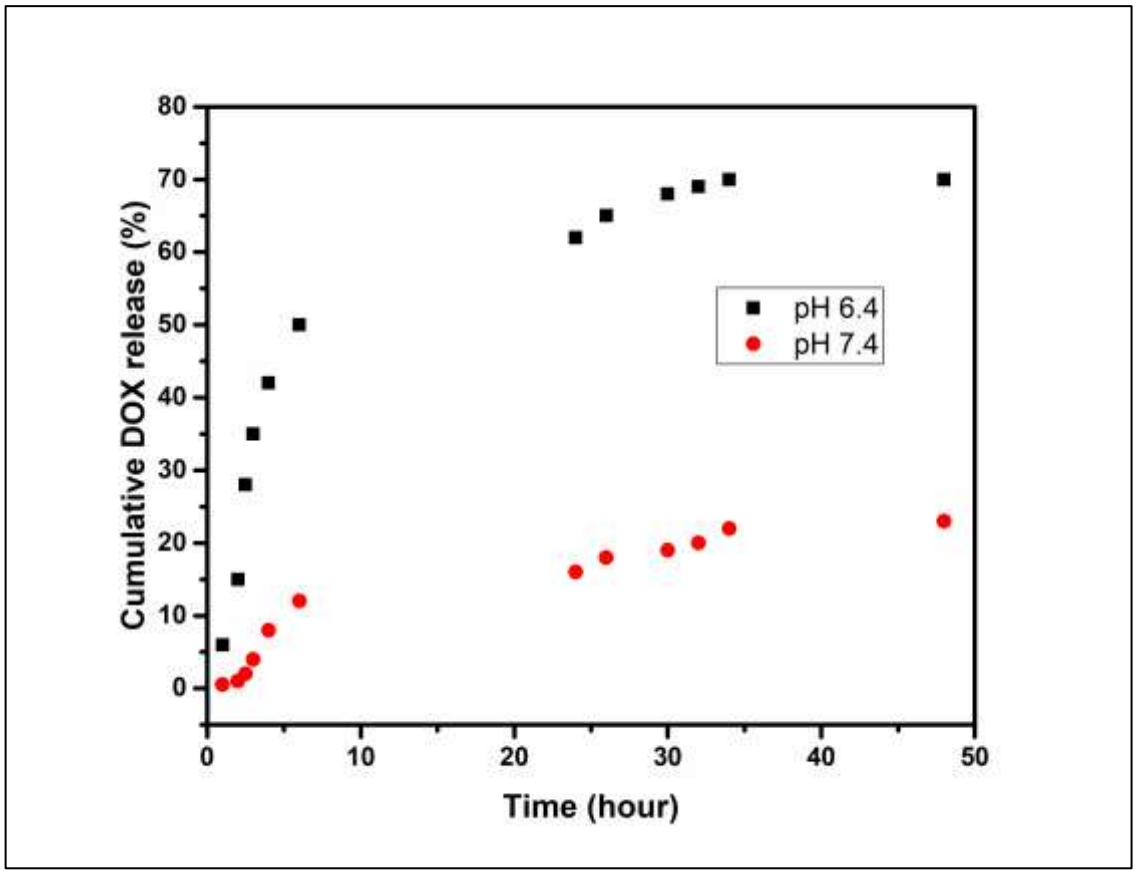

Figure 20: *Releasing curve of DOXO loaded on Cell-A at pH 6.4 and 7.4.*

The cumulative release study shows that the DOXO-loaded modified polymer has a clearly pH-dependent release behavior. As shown in Figure 20, at all time points, drug release at pH 6.4 is significantly higher than at pH 7.4. Initially, the burst release at pH 6.4 in the very early time, 1-6 hours, which reached 50.1% compared to 13.2% at pH 7.4 at the same interval. After the initial stage, the two systems showed a gradual, sustained release, with the one at a lower pH having a better slow release, increasing from 50.1% at 6 hours to 67.84% at 48 hours and This indicates continuous diffusion of DOXO from the polymer matrix, while at 7.4, the percentage jumped from 13.2% to 20.94% at the same intervals, suggesting that the polymer is less swollen and more stable at the normal cell's pH.

3.5 Preparation and characterization of cellulose hydrazone (Cell-HD)

The preparation of Cell-HD was performed by reacting hydrazine with Cell-A in a 2:2 mole ratio of hydrazine per anhydroglucose repeat unit. Hydrazine is a difunctional amino compound. The reaction is a condensation reaction in which the amine group of the hydrazine forms an imine linkage with Cell-A, as shown in Figure 21, with the loss of water molecules. The amino groups may interact with doxorubicin via physical interaction (H-bonding) and by forming an imine linkage, as shown in Figure 21.

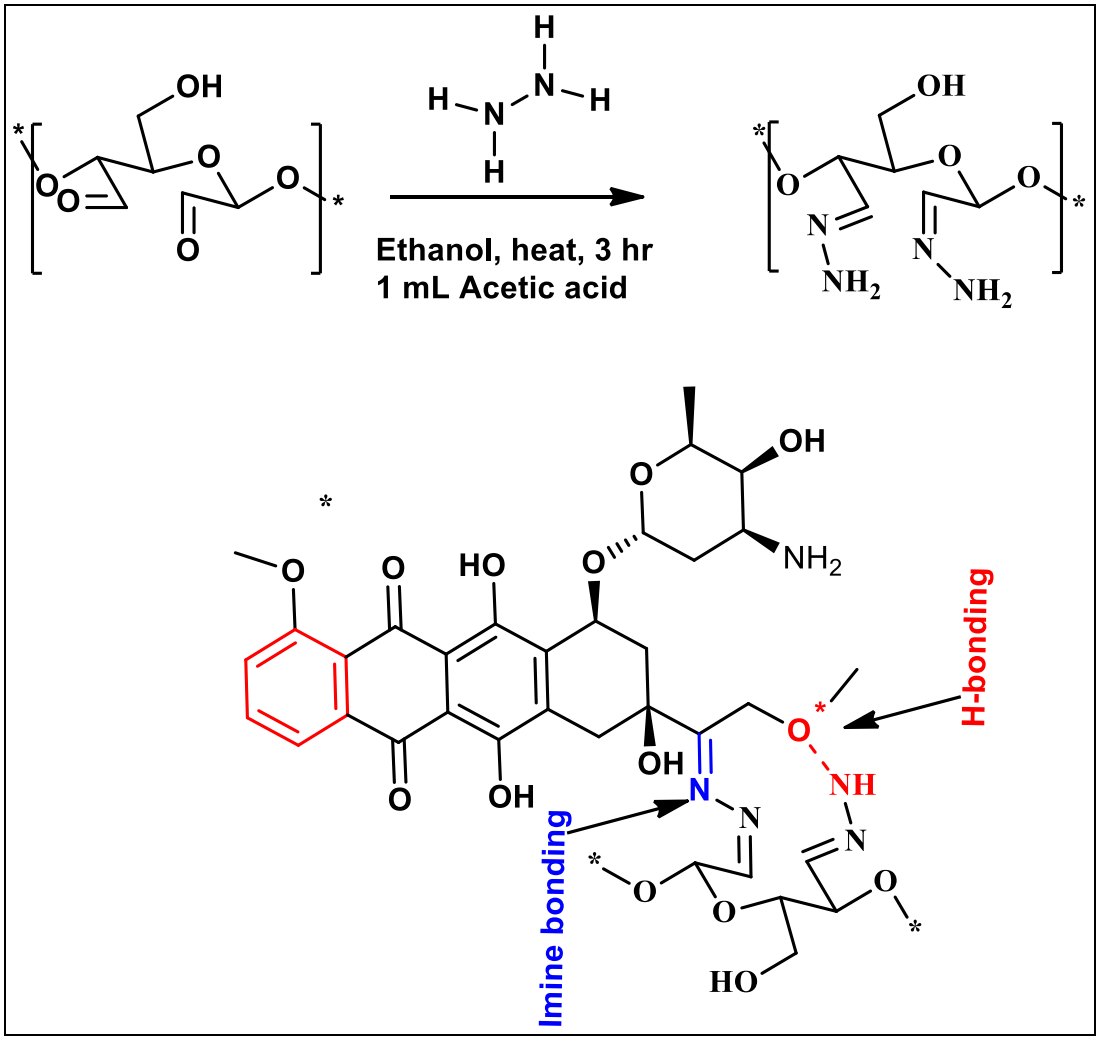

Figure 21: *Scheme for forming Cell-HD, and the possible ways of interaction with DOXO.*

3.5.1 Infrared spectrum of Cell-HD

The Schiff-base–type condensation of the dialdehyde on C2 and C3 with the amine group of the hydrazine forms the hydrazone group –C=N–NH_2.

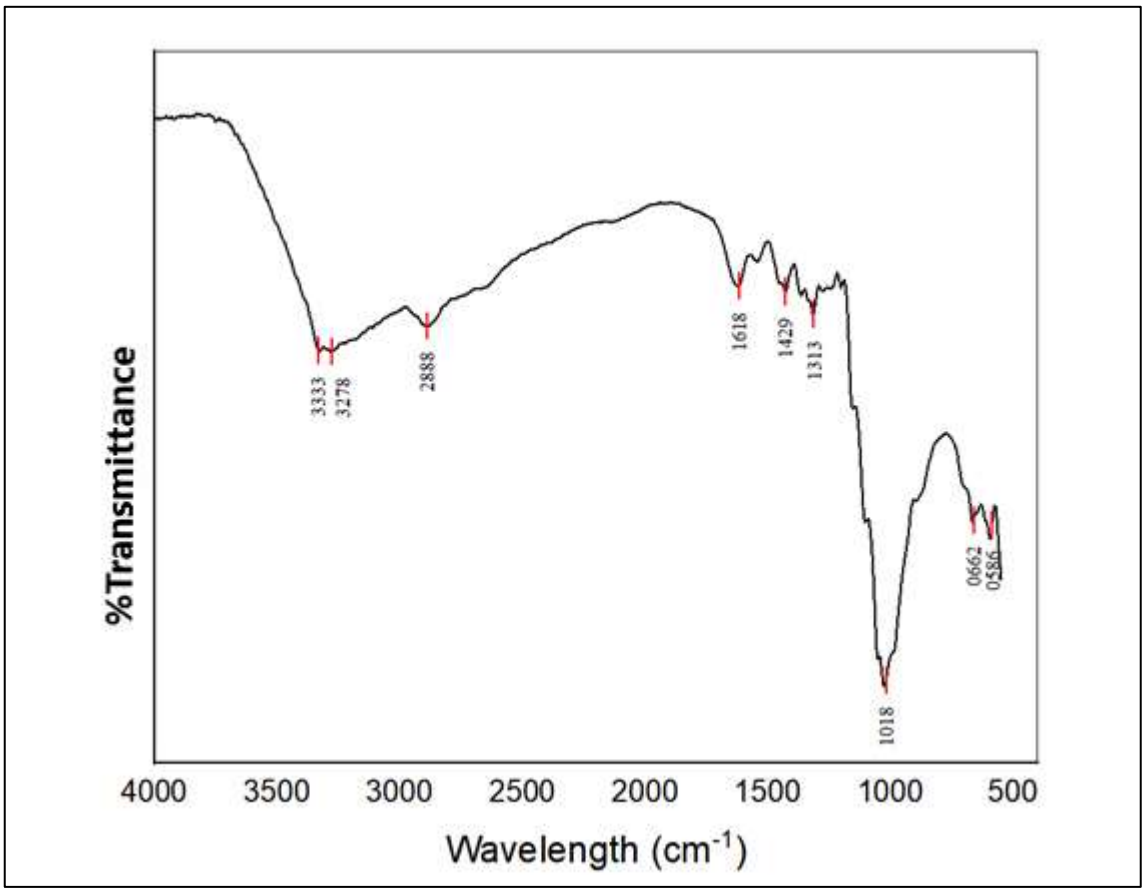

Figure 22: *IR spectrum of the Cellulose hydrazone.*

The IR shows a strong and broad peak at 3278 cm^{-1}, corresponding to the hydroxyl group of cellulose, which overlaps with the amine group of the hydrazone linkages formed at 3333 cm^{-1}, while the peak at 1618 cm^{-1} corresponds to the formation of C=N.

3.5.2 pH-dependent release study of DOXO loaded on Cell-HD

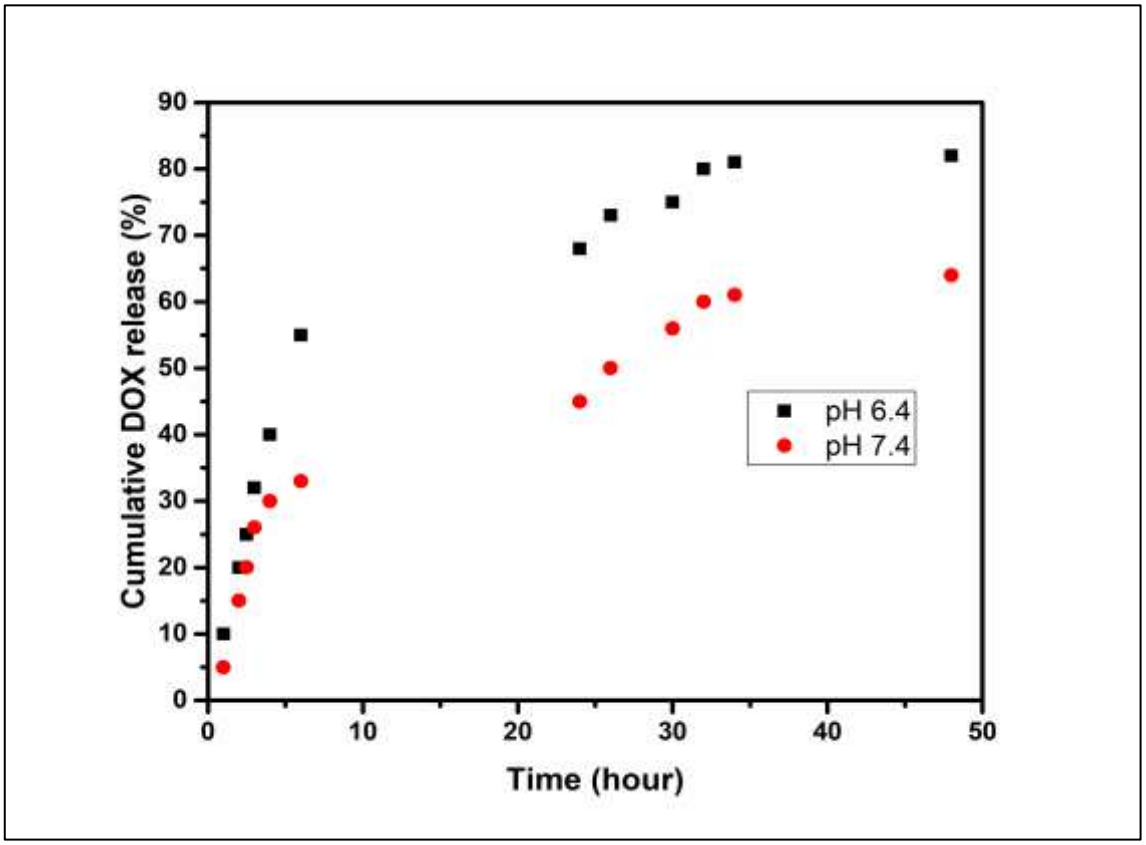

Figure 23*: Release amount of DOXO loaded on Cell-HD at pH 7.4. and pH 6.4.*

The slow-release test over 48 hours was performed. The amount of drug released at pH 6.4 is consistently higher than at pH 7.4. At first, in the 6 hours of the test, a burst release occurs at the two levels of pH. At pH 6.4, the percentage released is 55.17%, which is significantly higher than the 33.19% at pH 7.4. The burst release may indicate the ease of the chemical reaction in hydrolysis of the imine bond, the weakness of surface-adsorbed DOX molecules, or rapid diffusion of drug molecules near the polymer surface. After the sixth hour, the two systems showed a gradual and sustained release to reach 81.88% of the loaded amount at pH 6.4, while at 7.4 reached 64.46%.

3.6 Cytotoxicity

The in vitro cytotoxic activities of two novel drug delivery systems, Cell.A and Cell.HD loaded with DOXO was evaluated alongside free DOXO as a positive control. The evaluations were performed across six concentrations (0.02 to 80 µg/ml) against three human cancer cell lines: HepG-2, HeLa, and MCF-7. All systems showed a classic dose-dependent cytotoxicity profile.

In the HepG-2 cell line, Cell.A showed impressive potency, particularly at the intermediate threshold of 0.2 µg/ml, cell viability at 0.2 µg/ml reduced to 19%, greater than the standard chemotherapeutic agent DOXO, which retained 28% viability. While Cell.HD was less effective at lower doses, maintaining 55% cell viability at 0.2 µg/ml.

The HeLa cell line was slightly more flexible to low concentrations of the tested systems compared to HepG-2, though it succumbed rapidly at concentrations of 2 µg/ml and above. At 0.2 µg/ml DOXO and Cell.A showed highly similar activities, leaving 29% and 32% viable cells, respectively. While the Cell.HD again held back behind in potency at this concentration, showing a much higher viability of 61%.

The MCF-7 cell line showed a unique sensitivity profile, particularly regarding the performance of Cell.HD. At 0.2 µg/ml, moderate toxicity was shown by DOXO and Cell.A, 58%, 50%, respectively. Weak toxicity is shown by the Cell.HD at this concentration. But at 2 µg/ml Cell.HD demonstrated a massive cytotoxic surge, dropping cell viability sharply from 83% down to just 6%. As shown in Figures 24,25,26.

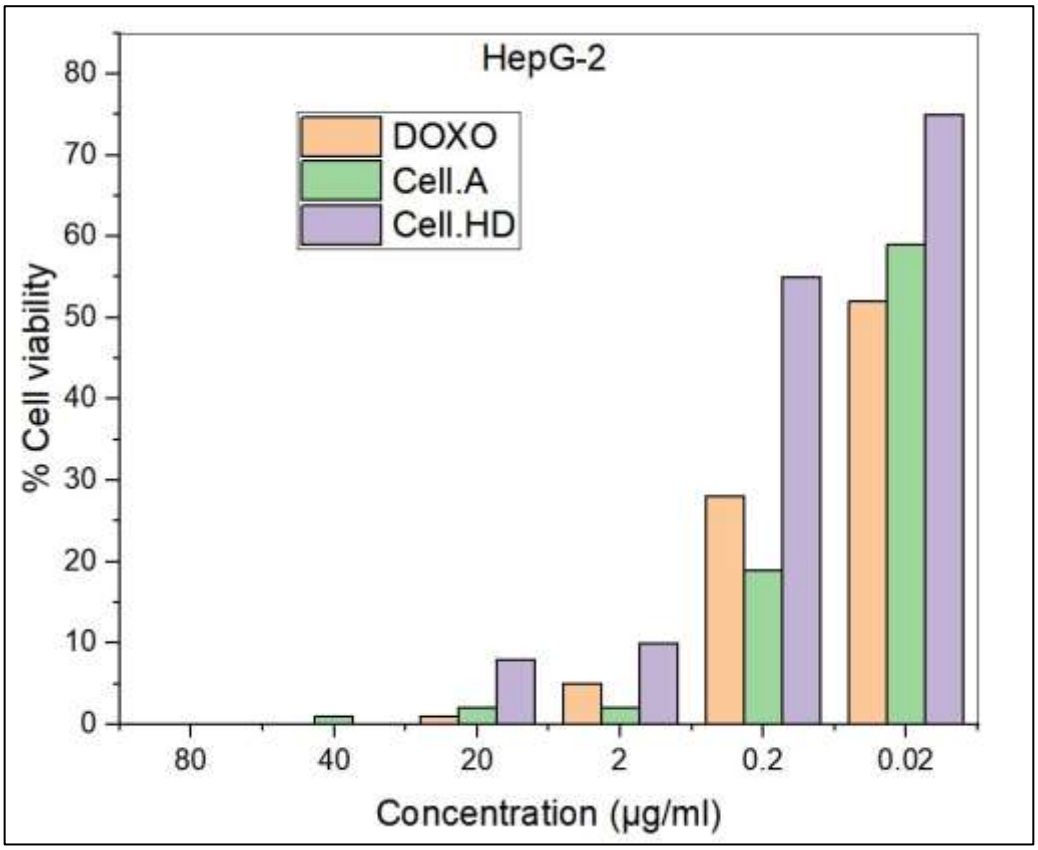

Figure 24: *%Cell viability at HepG-2 Cell line at different Concentrations.*

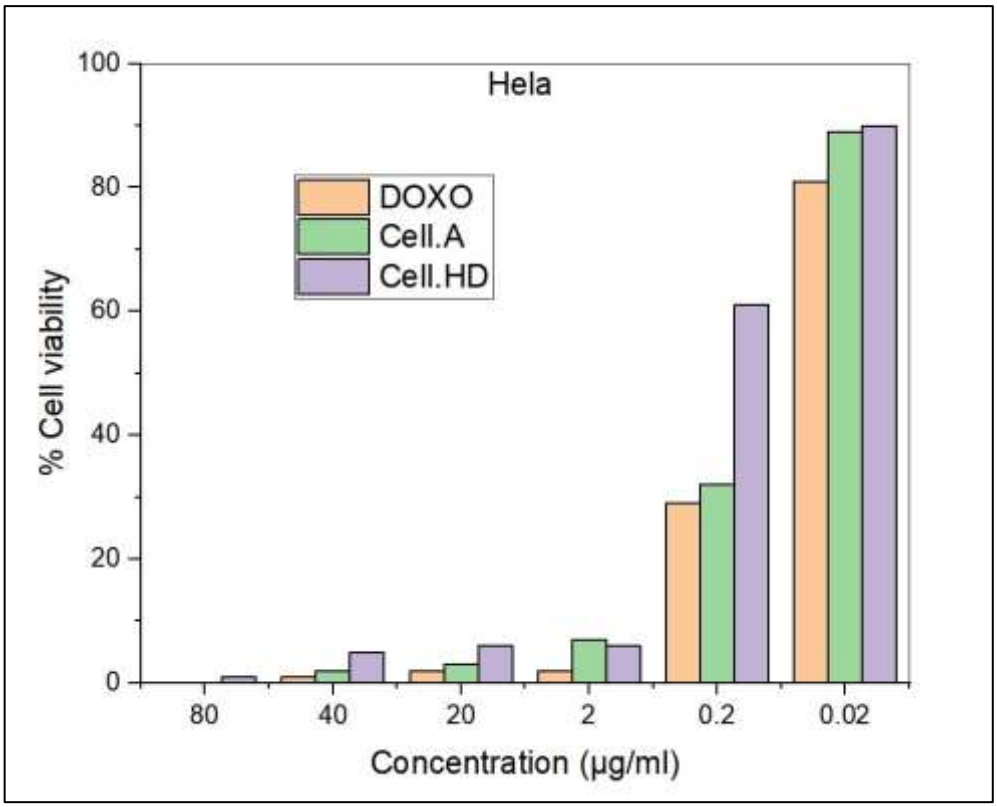

Figure 25*: %Cell viability at HeLa Cell line at different Concentrations.*

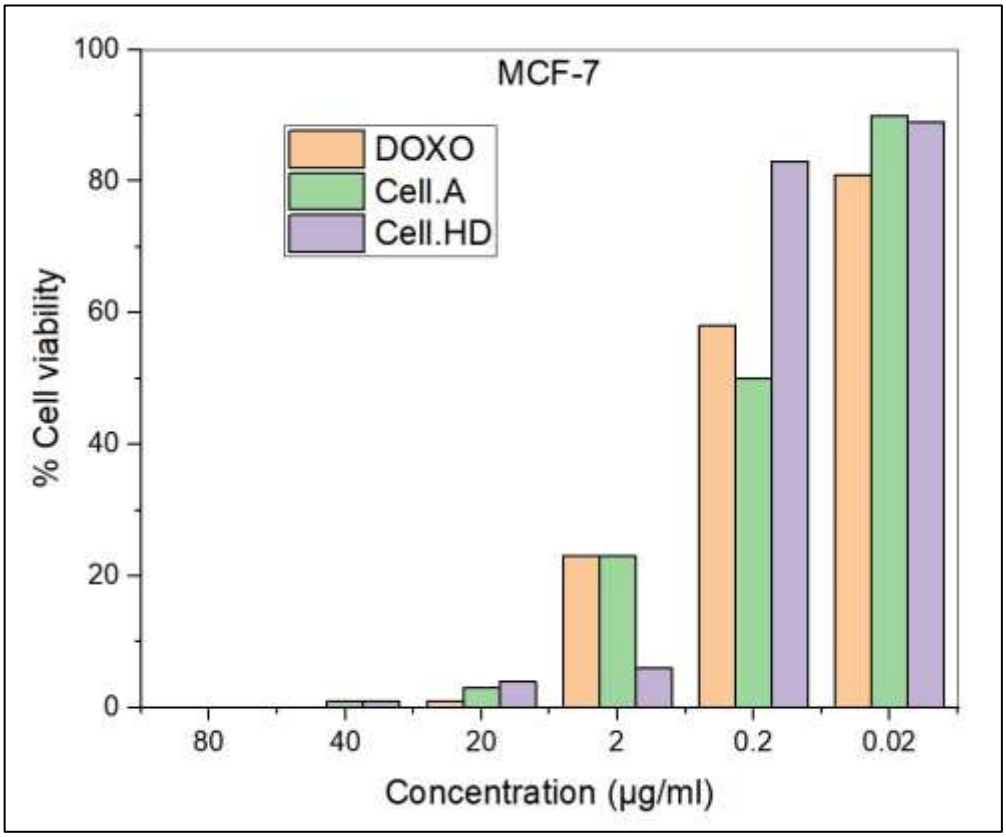

Figure 26: *%Cell viability at MCF-7 Cell line at different Concentrations.*

3.7 Characterization of CELL-A-Cysteine

3.7.1 Infrared Ft-IR

The condensation reaction of the aldehyde groups and the amine group produces an imine group. Leaving a free thiol and carboxyl, and depending on the hydrogen bonding with the anticancer drugs.

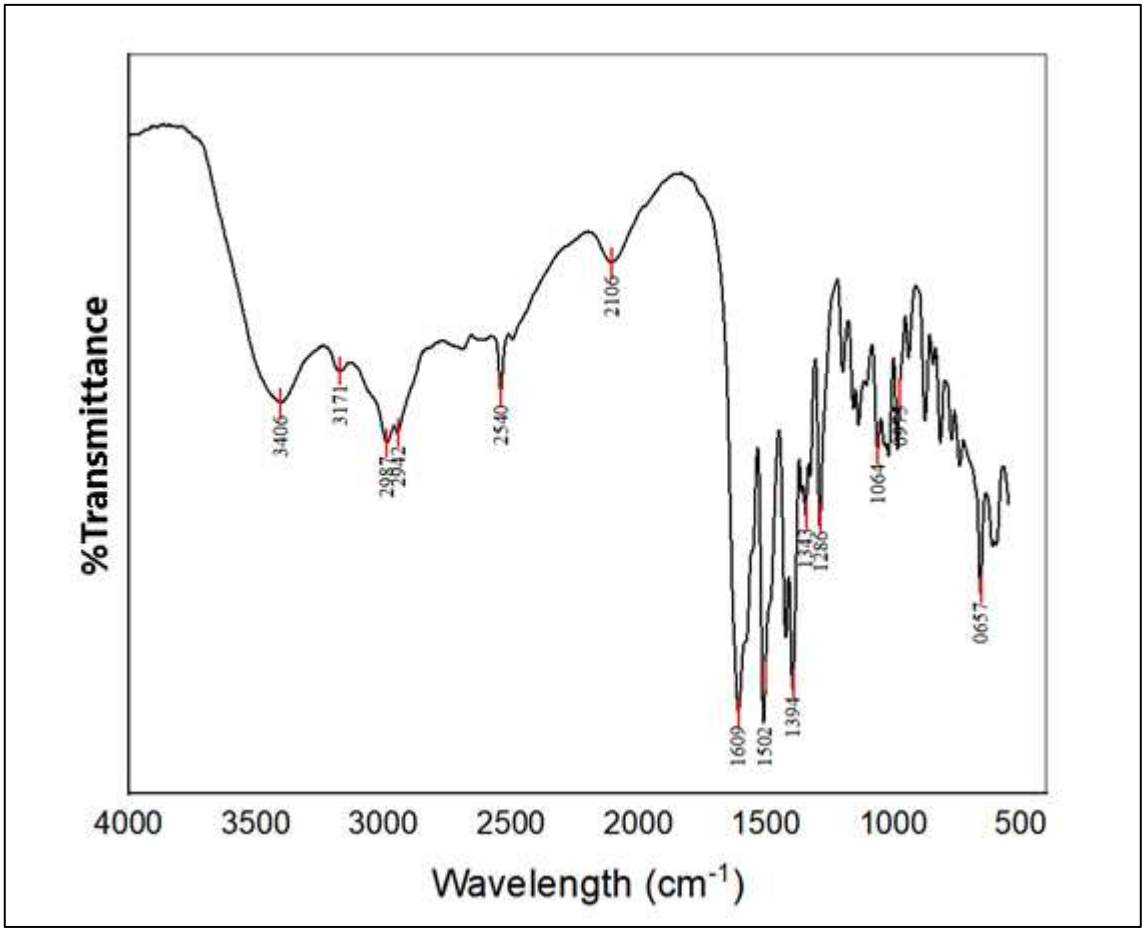

Figure 27*: The IR spectrum of Cell-A-Cysteine.*

The broad and intense peak at 3407 cm^{-1} corresponds to the O-H stretch of the cellulose backbone, confirming that the polysaccharide structure is untouched, and also overlaps with the carboxylic acid COOH group. The 2928 cm^{-1} peak represents the C-H, and the free S-H peak is at 2541 cm^{-1}. The peak at 1600 cm^{-1} is strong evidence for the C=N (imine) stretch of the Schiff base. The peak at 1510 cm^{-1} is for the asymmetric stretching of the carboxylate.

3.8 Conclusion

Several modified cellulose-based polymers were synthesized and characterized for use as pH-responsive drug delivery systems in cancer therapy. Cellulose was effectively modified through different mechanisms, including Tosylation, followed by nucleophilic substitution with amines (cysteine, melamine, p-phenylenediamine) to establish groups such as thiols and imines; oxidation to DAC; and modification to Cell-HD using hydrazine. Each modification was analyzed by FT-IR to confirm the reaction. Cell-Cys Nanoparticles were successfully produced with an optimal size for therapeutic delivery (70–90 nm), and sufficient repulsive forces were ensured by a negative zeta potential of -28 mV, preventing aggregation and maintaining suspension stability. Modified polymers showed a clear pH-responsive release profile. The polymer framework successfully traps the drugs at the physiological pH (7.4), while showing a rapid release in acidic environments (pH 6.4–6.5). A biphasic pattern was observed in each release profile, with an initial burst release of surface-associated drug followed by sustained, controlled diffusion from the polymer matrix. through mechanisms such as increased polymer swelling, protonation of imine bonds, and disruption of hydrogen bonding between the matrix and the drug. Cell-A and Cell-HD carriers showed high therapeutic potential by inhibiting cancer cell growth. Specifically, the Cell-A carrier loaded with DOXO showed results very similar to those of the free drug in terms of cytotoxicity against HepG-2 liver cancer cells. 100% cell inhibition was achieved across several cell lines, including MCF-7 and HeLa. In summary, the modified polymers framework provides a balance between potent efficacy and stability in healthy tissues within the tumor microenvironment, reducing the systemic side effects typically associated with chemotherapy.

References

1. Filho, A.M., et al., *The GLOBOCAN 2022 cancer estimates: Data sources, methods, and a snapshot of the cancer burden worldwide.* International Journal of Cancer, 2025. 156(7): p. 1336-1346.

2. Meacham, C.E. and S.J. Morrison, *Tumour heterogeneity and cancer cell plasticity.* Nature, 2013. 501(7467): p. 328-337.

3. Belpomme, D., et al., *The growing incidence of cancer: Role of lifestyle and screening detection (Review).* Int J Oncol, 2007. 30(5): p. 1037-1049.

4. Kasheverov, I.E., et al., *α-Conotoxin GI benzoylphenylalanine derivatives.* The FEBS Journal, 2006. 273(7): p. 1373-1388.

5. Mills, P.K., *Response to "Commentary on 'Agricultural exposures and gastric cancer risk in Hispanic farm workers in California'": (P.K. Mills, R.C. Yang, Environ. Res. 104 (2007) 282–289).* Environmental Research, 2007. 105(2): p. 287-288.

6. Danaei, G., et al., *Causes of cancer in the world: comparative risk assessment of nine behavioural and environmental risk factors.* The Lancet, 2005. 366(9499): p. 1784-1793.

7. Newby, J.A. and C. Vyvyan Howard, *Environmental influences in cancer aetiology.* Journal of Nutritional & Environmental Medicine, 2005. 15(2-3): p. 56-114.

8. Zafar, A., et al., *Advancements and limitations in traditional anti-cancer therapies: a comprehensive review of surgery, chemotherapy, radiation therapy, and hormonal therapy.* Discover Oncology, 2025. 16.

9. Anand, U., et al., *Cancer chemotherapy and beyond: Current status, drug candidates, associated risks and progress in targeted therapeutics.* Genes & Diseases, 2022. 10: p. 1367-1401.

10. Frank, S., *How cancer arises: Genetics releases, plasticity creates, genetics stabilizes.* Proceedings of the National Academy of Sciences of the United States of America, 2025. 122.

11. Gong, Q., et al., *Recent advances of anti-tumor nano-strategies via overturning pH gradient: alkalization and acidification.* Journal of Nanobiotechnology, 2025. 23.

12. Kato, Y., et al., *Acidic extracellular microenvironment and cancer.* Cancer Cell International, 2013. 13: p. 89-89.

13. Feng, Q., et al., *Severely polarized extracellular acidity around tumour cells.* Nature Biomedical Engineering, 2024. 8: p. 787-799.

14. Mishra, S., et al., *Transmembrane pH gradient imaging in rodent glioma models.* NMR in Biomedicine, 2024. 37.

15. Boedtkjer, E. and S. Pedersen, *The Acidic Tumor Microenvironment as a Driver of Cancer.* Annual review of physiology, 2019.

16. Persi, E., et al., *Systems analysis of intracellular pH vulnerabilities for cancer therapy.* Nature Communications, 2018. 9.

17. Bukowski, K., M. Kciuk, and R. Kontek, *Mechanisms of Multidrug Resistance in Cancer Chemotherapy.* International Journal of Molecular Sciences, 2020. 21.

18. Castañeda, A.M., C. Meléndez, D. Uribe, and J. Pedroza-Díaz, *Synergistic effects of natural compounds and conventional chemotherapeutic agents: recent insights for the development of cancer treatment strategies.* Heliyon, 2022. 8.

19. Gilad, Y., G. Gellerman, D. Lonard, and B. O'Malley, *Drug Combination in Cancer Treatment—From Cocktails to Conjugated Combinations.* Cancers, 2021. 13.

20. Li, B., et al., *Nano-drug co-delivery system of natural active ingredients and chemotherapy drugs for cancer treatment: a review.* Drug Deliv, 2022. 29(1): p. 2130-2161.

21. Tímár, J. and A. Uhlyarik, *On-Target Side Effects of Targeted Therapeutics of Cancer.* Pathol Oncol Res, 2022. 28: p. 1610694.

22. Gooneh-Farahani, S., S.M. Naghib, M.R. Naimi-Jamal, and A. Seyfoori, *A pH-sensitive nanocarrier based on BSA-stabilized graphene-chitosan nanocomposite for sustained and prolonged release of anticancer agents.* Sci Rep, 2021. 11(1): p. 17404.

23. Joo, J.Y., G.Y. Park, and S.S.A. An, *Biocompatible and biodegradable fibrinogen microspheres for tumor-targeted doxorubicin delivery.* International Journal of Nanomedicine, 2015. 10(sup1): p. 101-111.

24. Chen, J., et al., *Research progress in lignin-based slow/controlled release fertilizer.* ChemSusChem, 2020. 13(17): p. 4356-4366.

25. Ashrafizadeh, M., et al., *(Nano) platforms in breast cancer therapy: drug/gene delivery, advanced nanocarriers and immunotherapy.* Medicinal Research Reviews, 2023. 43(6): p. 2115-2176.

26. Klemm, D., et al., *Comprehensive cellulose chemistry. Volume 1: Fundamentals and analytical methods*. 1998.

27. Ferro, M., et al., *An Integrated Approach to Optimizing Cellulose Mercerization.* Polymers, 2020. 12.

28. Da Silva Perez, D., S. Montanari, and M. Vignon, *TEMPO-mediated oxidation of cellulose III.* Biomacromolecules, 2003. 4 5: p. 1417-1425.

29. Loeb, L. and L. Segal, *Preparation of cotton cellulose IV from cotton cellulose III.* Journal of Polymer Science, 1954. 14: p. 121-123.

30. Swingler, S., et al., *Recent Advances and Applications of Bacterial Cellulose in Biomedicine.* Polymers, 2021. 13.

31. Wahid, F., et al., *Bacterial cellulose and its potential for biomedical applications.* Biotechnology advances, 2021: p. 107856.

32. Picheth, G., et al., *Bacterial cellulose in biomedical applications: A review.* International journal of biological macromolecules, 2017. 104 Pt A: p. 97-106.

33. Edgar, K.J., et al., *Advances in cellulose ester performance and application.* Progress in polymer science, 2001. 26(9): p. 1605-1688.

34. You, J., et al., *Mild, rapid and efficient etherification of cellulose.* Cellulose, 2022. 29: p. 9583-9596.

35. Pinto, E., et al., *Cellulose Processing from Biomass and its Derivatization into Carboxymethylcellulose: A Review.* Scientific African, 2021.

36. Padmanabhan, S.K., et al., *Carboxymethylcellulose-Based Hydrogel Obtained from Bacterial Cellulose.* Molecules, 2023. 28.

37. Kim, J., et al., *Cellulose Etherification with Glycidol for Aqueous Rheology Modification.* ACS Applied Polymer Materials, 2024.

38. Wang, Y., X. Wang, Y. Xie, and K. Zhang, *Functional nanomaterials through esterification of cellulose: a review of chemistry and application.* Cellulose, 2018. 25: p. 3703-3731.

39. Liu, S., et al., *Esterification of cellulose using carboxylic acid-based deep eutectic solvents to produce high-yield cellulose nanofibers.* Carbohydrate polymers, 2021. 251: p. 117018.

40. Duceac, I., F. Tanasă, and S. Coseri, *Selective Oxidation of Cellulose—A Multitask Platform with Significant Environmental Impact.* Materials, 2022. 15.

41. Coseri, S., et al., *Oxidized cellulose--survey of the most recent achievements.* Carbohydrate polymers, 2013. 93 1: p. 207-215.

42. Coseri, S., *Cellulose: To depolymerize… or not to?* Biotechnology advances, 2017. 35 2: p. 251-266.

43. Mendoza, D., et al., *One-shot TEMPO-periodate oxidation of native cellulose.* Carbohydrate polymers, 2019. 226: p. 115292.

44. Patterson, G. and Y. Hsieh, *Tunable dialdehyde/dicarboxylate nanocellulosess by stoichiometrically optimized sequential periodate–chlorite oxidation for tough and wet shape recoverable aerogels.* Nanoscale Advances, 2020. 2: p. 5623-5634.

45. Sirviö, J., et al., *Periodate oxidation of cellulose at elevated temperatures using metal salts as cellulose activators.* Carbohydrate Polymers, 2011. 83: p. 1293-1297.

46. Dang, X., et al., *Production and characterization of dialdehyde cellulose through green and sustainable approach.* Cellulose, 2019. 26: p. 9503-9515.

47. Singam, A., N. Killi, P. Patel, and R. Gundloori, *PEGylated ethyl cellulose micelles as a nanocarrier for drug delivery.* RSC Advances, 2021. 11: p. 30532-30543.

48. Wang, H., et al., *Nano micelles of cellulose-graft-poly (l-lactic acid) anchored with epithelial cell adhesion antibody for enhanced drug loading and anti-tumor effect.* Materials today communications, 2020. 22: p. 100764.

49. Krasnopeeva, E., et al., *Poly(methacrylic Acid)-Cellulose Brushes as Anticancer Porphyrazine Carrier.* Nanomaterials, 2021. 11.

50. Munawaroh, H.S.H., et al., *Bacterial cellulose nanocrystal as drug delivery system for overcoming the biological barrier of cyano-phycocyanin: a biomedical application of microbial product.* Bioengineered, 2023. 14.

51. Ali, I., et al., *Reduction-responsive and bioorthogonal carboxymethyl cellulose based soft hydrogels cross-linked via IEDDA click chemistry for cancer therapy application.* International journal of biological macromolecules, 2022.

52. Pooresmaeil, M. and H. Namazi, *Folic acid-modified photoluminescent dialdehyde carboxymethyl cellulose crosslinked bionanogels for pH-controlled and tumor-targeted co-drug delivery.* International journal of biological macromolecules, 2022.

53. Shaker, L., A. Al-Amiery, and A. Kadhum, *Advances in Drug Delivery Systems: A Mini-Review.* Al-Ameed Journal for Medical Research and Health Sciences, 2023.

54. Homayun, B., X. Lin, and H.-J. Choi, *Challenges and Recent Progress in Oral Drug Delivery Systems for Biopharmaceuticals.* Pharmaceutics, 2019. 11.

55. Bhutani, U., T. Basu, and S. Majumdar, *Oral drug delivery: Conventional to Long Acting New-Age Designs.* European journal of pharmaceutics and biopharmaceutics : official journal of Arbeitsgemeinschaft fur Pharmazeutische Verfahrenstechnik e.V, 2021.

56. Liu, D., F. Yang, F. Xiong, and N. Gu, *The Smart Drug Delivery System and Its Clinical Potential.* Theranostics, 2016. 6: p. 1306-1323.

57. Javanbakht, S. and A. Shaabani, *Carboxymethyl cellulose-based oral delivery systems.* International journal of biological macromolecules, 2019. 133: p. 21-29.

58. Gong, J., et al., *A review of recent advances of cellulose-based intelligent-responsive hydrogels as vehicles for controllable drug delivery system.* International journal of biological macromolecules, 2024: p. 130525.

59. Huo, Y., et al., *Nanocelluloses-Based Composite Materials Used in Drug Delivery Systems.* Polymers, 2022. 14.

60. Ciolacu, D., R. Nicu, and F. Ciolacu, *Cellulose-Based Hydrogels as Sustained Drug-Delivery Systems.* Materials, 2020. 13.

61. Kupnik, K., M. Primožič, V. Kokol, and M. Leitgeb, *Nanocelluloses in Drug Delivery and Antimicrobially Active Materials.* Polymers, 2020. 12.

62. Selim, S., M. Almuhayawi, S.A. Jaouni, and M. Harun-Ur-Rashid, *Synthetic biology innovations in designing cellulose-based smart drug delivery systems.* BioResources, 2025.

63. Alam, A., P. Kalyani, A. Khan, and M. Khandelwal, *Bacterial cellulose in transdermal drug delivery systems: Expanding horizons in multi-scale therapeutics and patient-centric approach.* International journal of pharmaceutics, 2025: p. 125254.

64. Wang, K., Y. Wu, J. Remón, and W. Ding, *Recent advances in versatile cellulose-based 3D-printed drug delivery systems: A review.* International journal of biological macromolecules, 2025: p. 144433.

65. Khan, S., et al., *A review on nanotechnology: Properties, applications, and mechanistic insights of cellular uptake mechanisms.* Journal of Molecular Liquids, 2021.

66. Sher, E.K., et al., *Nanotechnology in medicine revolutionizing drug delivery for cancer and viral infection treatments.* International journal of pharmaceutics, 2024: p. 124345.

67. Sheikhi, A., et al., *Recent advances in nanoengineering cellulose for cargo delivery.* Journal of controlled release : official journal of the Controlled Release Society, 2019. 294: p. 53-76.

68. Gunathilake, T.S.U., et al., *Recent advances in celluloses and their hybrids for stimuli-responsive drug delivery.* International journal of biological macromolecules, 2020.

69. Feng, S., et al., *Amidated Pectin/Nanocelluloses Hybrid Cryogel System with a pH-Responsive Release Profile for Small Intestinal Delivery.* Gels, 2025. 11.

70. Hujaya, S., G. Lorite, S. Vainio, and H. Liimatainen, *Polyion complex hydrogels from chemically modified cellulose nanofibrils: Structure-function relationship and potential for controlled and pH-responsive release of doxorubicin.* Acta biomaterialia, 2018. 75: p. 346-357.

71. Liu, Z., et al., *Temperature/pH-Responsive Carboxymethyl Cellulose/Poly (N-isopropyl acrylamide) Interpenetrating Polymer Network Aerogels for Drug Delivery Systems.* Polymers, 2022. 14.

72. Young, S., et al., *Engineering hairy cellulose nanocrystals for chemotherapy drug capture.* Materials today. Chemistry, 2022. 23.

73. Andrade, F., et al., *Stimuli-Responsive Hydrogels for Cancer Treatment: The Role of pH, Light, Ionic Strength and Magnetic Field.* Cancers, 2021. 13.

74. Gülçelik, N., K.N. Çifci, and N. Alemdar, *The effect of sulfonated reduced graphene oxide on the properties of ionic strength sensitive PEC film comprising protein/polysaccharides combined system.* International journal of biological macromolecules, 2024: p. 136490.

75. Yu, B., B. Choi, W. Li, and D.H. Kim, *Magnetic field boosted ferroptosis-like cell death and responsive MRI using hybrid vesicles for cancer immunotherapy.* Nature Communications, 2020. 11.

76. Ge, M., et al., *Magnetostrictive-Piezoelectric-Triggered Nanocatalytic Tumor Therapy.* Nano letters, 2021.

77. Li, D., et al., *Elongated Magnetic Nanorobots with Multi-Enzymatic Cascades for Active In Vivo Tumor Targeting and Enhanced Chemodynamic Therapy.* ACS nano, 2025.

78. Zhu, J., et al., *Dual Responsive Magnetic Drug Delivery Nanomicelles with Tumor Targeting for Enhanced Cancer Chemo/Magnetothermal Synergistic Therapy.* International Journal of Nanomedicine, 2023. 18: p. 7647-7660.

79. Poole, L., *The basics of thiols and cysteines in redox biology and chemistry.* Free radical biology & medicine, 2015. 80: p. 148-157.

80. Sritharan, S. and N. Sivalingam, *A comprehensive review on time-tested anticancer drug doxorubicin.* Life sciences, 2021: p. 119527.

81. Van Der Zanden, S., X. Qiao, and J. Neefjes, *New insights into the activities and toxicities of the old anticancer drug doxorubicin.* The Febs Journal, 2020. 288: p. 6095-6111.

82. Zhang, J., et al., *Effectiveness and safety of pegylated liposomal doxorubicin versus epirubicin as neoadjuvant or adjuvant chemotherapy for breast cancer: a real-world study.* BMC Cancer, 2021. 21.

83. Gautam, S., et al., *Recent doxorubicin-conjugates in cancer drug delivery: Exploring conjugation strategies for enhanced efficacy and reduced toxicity.* International journal of pharmaceutics, 2025: p. 125556.

84. Denel-Bobrowska, M. and A. Marczak, *Structural modifications in the sugar moiety as a key to improving the anticancer effectiveness of doxorubicin.* Life sciences, 2017. 178: p. 1-8.

85. Tempel, M., et al., *Doxorubicin, a DNA intercalator, inhibits transcription elongation.* Biochemistry and cell biology = Biochimie et biologie cellulaire, 2025.

86. Pérez-Arnaiz, C., N. Busto, J. Leal, and B. García, *New insights into the mechanism of the DNA/doxorubicin interaction.* The journal of physical chemistry. B, 2014. 118 5: p. 1288-1295.

87. Nedělníková, A., et al., *Atomistic Insights Into Interaction of Doxorubicin With DNA: From Duplex to Nucleosome.* Journal of Computational Chemistry, 2025. 46.

88. Lee, J., M.K. Choi, and I. Song, *Recent Advances in Doxorubicin Formulation to Enhance Pharmacokinetics and Tumor Targeting.* Pharmaceuticals, 2023. 16.

89. Mohajeri, M. and A. Sahebkar, *Protective effects of curcumin against doxorubicin-induced toxicity and resistance: A review.* Critical reviews in oncology/hematology, 2018. 122: p. 30-51.

90. Mirzaei, S., et al., *Nrf2 Signaling Pathway in Chemoprotection and Doxorubicin Resistance: Potential Application in Drug Discovery.* Antioxidants, 2021. 10.

91. Chegaev, K., et al., *H2S-Donating Doxorubicins May Overcome Cardiotoxicity and Multidrug Resistance.* Journal of medicinal chemistry, 2016. 59 10: p. 4881-4889.

92. Vincenzi, M., et al., *Identification of prokineticin-2 as potential pharmacodynamic biomarker for overcoming doxorubicin resistance in multicellular breast cancer spheroids.* British journal of pharmacology, 2025.

93. Ibrahim, M., et al., *Encapsulation, Release, and Cytotoxicity of Doxorubicin Loaded in Liposomes, Micelles, and Metal-Organic Frameworks: A Review.* Pharmaceutics, 2022. 14.

94. Mahani, M., et al., *Doxorubicin delivery to breast cancer cells with transferrin-targeted carbon quantum dots: An in vitro and in silico study.* Journal of Drug Delivery Science and Technology, 2021. 62: p. 102342.

95. Akhtar, N., et al., *SPIONs Conjugate Supported Anticancer Drug Doxorubicin's Delivery: Current Status, Challenges, and Prospects.* Nanomaterials, 2022. 12.

96. Almajidi, Y., et al., *Doxorubicin-loaded micelles in tumor cell specific chemotherapy.* Environmental research, 2023: p. 115722.

97. Cacicedo, M., et al., *Modified bacterial cellulose scaffolds for localized doxorubicin release in human colorectal HT-29 cells.* Colloids and surfaces. B, Biointerfaces, 2016. 140: p. 421-429.

98. Chen, N., et al., *Cellulose-based injectable hydrogel composite for pH-responsive and controllable drug delivery.* Carbohydrate polymers, 2019. 225: p. 115207.

99. Wang, H., et al., *A new pathway towards polymer modified cellulose nanocrystals via a "grafting onto" process for drug delivery.* Polymer Chemistry, 2015. 6: p. 4206-4209.

100. Gholamali, I. and M. Yadollahi, *Doxorubicin-loaded carboxymethyl cellulose/Starch/ZnO nanocomposite hydrogel beads as an anticancer drug carrier agent.* International journal of biological macromolecules, 2020.

101. Ulusoy, H. and N. Sanlier, *A minireview of quercetin: from its metabolism to possible mechanisms of its biological activities.* Critical Reviews in Food Science and Nutrition, 2020. 60: p. 3290-3303.

102. Aghababaei, F. and M. Hadidi, *Recent Advances in Potential Health Benefits of Quercetin.* Pharmaceuticals, 2023. 16.

103. Carrillo-Martinez, E.J., et al., *Quercetin, a Flavonoid with Great Pharmacological Capacity.* Molecules, 2024. 29.

104. Biswas, P., et al., *A Comprehensive Analysis and Anti-Cancer Activities of Quercetin in ROS-Mediated Cancer and Cancer Stem Cells.* International Journal of Molecular Sciences, 2022. 23.

105. Reyes-Farias, M. and C. Carrasco-Pozo, *The Anti-Cancer Effect of Quercetin: Molecular Implications in Cancer Metabolism.* International Journal of Molecular Sciences, 2019. 20.

106. Črnivec, I.G.O., et al., *Aspects of quercetin stability and its liposomal enhancement in yellow onion skin extracts.* Food chemistry, 2024. 459: p. 140347.

107. Qi, W., W. Qi, D. Xiong, and M. Long, *Quercetin: Its Antioxidant Mechanism, Antibacterial Properties and Potential Application in Prevention and Control of Toxipathy.* Molecules, 2022. 27.

108. Tiwari, S., Juhne, S. Rathod, and P. Bahadur, *Solubilization of quercetin in P123 micelles: Scattering and NMR studies.* Colloids and Surfaces A: Physicochemical and Engineering Aspects, 2021.

109. Liao, L.l., et al., *Dietary proteins as excipient ingredients for improving the solubility, stability, and bioaccessibility of quercetin: Role of intermolecular interactions.* Food research international, 2022. 161: p. 111806.

110. Xu, et al., *Superior solubility of anhydrous quercetin and polymer physical mixtures compared to amorphous solid dispersions.* RSC Advances, 2025. 15: p. 9348-9358.

111. Cao, H., et al., *Stability of quercetin in DMEM and cell culture with A549 cells.* eFood, 2022.

112. Li, M., et al., *Simple preparation and greatly improved oral bioavailability: The supersaturated drug delivery system of quercetin based on PVP K30.* Drug Delivery and Translational Research, 2024. 14: p. 3225-3238.

113. Tran, T.H., et al., *Quercetin-containing self-nanoemulsifying drug delivery system for improving oral bioavailability.* Journal of pharmaceutical sciences, 2014. 103 3: p. 840-852.

114. Münster, L., et al., *Stability and aging of solubilized dialdehyde cellulose.* Cellulose, 2017. 24.

Appendices

Appendix A

Tables

Table A.1: *Cell Viability and Inhibition of HepG-2 Cells Treated with Varying Concentrations of DOXO from Cell-A. Values represent a single experiment performed in duplicate*

HepG-2								
	negative control	80 µg/ml	40 µg/ml	20 µg/ml	2 µg/ml	0.2 µg/ml	0.02 µg/ml	blank
abs1	1.235	0.247	0.256	0.267	0.266	0.451	0.842	0.244
abs2	1.240	0.241	0.251	0.261	0.269	0.41	0.82	0.244
average of absorbance	1.238	0.244	0.254	0.264	0.268	0.431	0.831	0.244
average of absorbance - blank	0.994	0.000	0.010	0.020	0.024	0.187	0.587	0.000
cell viability %	100	0	1	2	2	19	59	0
cell inhibition %	0	100	99	98	98	81	41	100

Table A.2: *Cell Viability and Inhibition of HeLa Cells Treated with Varying Concentrations of DOXO from Cell-A. Values represent a single experiment performed in duplicate.*

HeLa								
	negative control	80 µg/ml	40 µg/ml	20 µg/ml	2 µg/ml	0.2 µg/ml	0.02 µg/ml	blank
abs1	0.952	0.242	0.254	0.263	0.294	0.463	0.882	0.244
abs2	0.927	0.244	0.256	0.261	0.293	0.468	0.84	0.244
average of absorbance	0.940	0.243	0.255	0.262	0.294	0.466	0.861	0.244
average of absorbance - blank	0.696	-0.001	0.011	0.018	0.050	0.222	0.617	0.000
cell viability %	100	0	2	3	7	32	89	0
cell inhibition %	0	100	98	97	93	68	11	100

Table A.3: *Cell Viability and Inhibition of MCF-7 Cells Treated with Varying Concentrations of DOXO from Cell-A. Values represent a single experiment performed in duplicate*

MCF-7								
	negative control	**80 µg/ml**	**40 µg/ml**	**20 µg/ml**	**2 µg/ml**	**0.2 µg/ml**	**0.02 µg/ml**	**blank**
abs1	**1.478**	**0.247**	**0.259**	**0.284**	**0.508**	**0.860**	**1.343**	**0.244**
abs2	**1.487**	**0.248**	**0.257**	**0.285**	**0.556**	**0.856**	**1.375**	**0.244**
average of absorbance	**1.483**	**0.248**	**0.258**	**0.285**	**0.532**	**0.858**	**1.359**	**0.244**
average of absorbance - blank	**1.239**	**0.004**	**0.014**	**0.041**	**0.288**	**0.614**	**1.115**	**0.000**
cell viability %	**100 ± 0.52%**	**0 ± 0.06%**	**1 ± 0.11%**	**3 ± 0.06%**	**23 ± 2.74%**	**50 ± 0.23%**	**90 ± 1.82%**	**0**
cell inhibition %	0	100	99	97	77	50	10	100

Table A4: *Cell Viability and Inhibition of LX-2 Cells Treated with Varying Concentrations of DOXO from Cell-A. Values represent a single experiment performed in duplicate*

LX-2								
	negative control	80 µg/ml	40 µg/ml	20 µg/ml	2 µg/ml	0.2 µg/ml	0.02 µg/ml	blank
abs1	1.108	0.297	0.360	0.4	0.482	0.661	0.722	0.244
abs2	1.105	0.267	0.343	0.403	0.473	0.687	0.754	0.244
average of absorbance	1.106	0.282	0.352	0.402	0.478	0.674	0.738	0.244
average of absorbance - blank	0.862	0.038	0.108	0.158	0.234	0.430	0.494	0.000
cell viability %	100	4	12	18	27	50	57	0
cell inhibition %	0	96	88	82	73	50	43	100

Table A.5: *Cell Viability and Inhibition of HepG-2 Cells Treated with Varying Concentrations of DOXO from Cell-Hydrazone. Values represent a single experiment performed in duplicate.*

HepG-2								
	negative control	80 µg/ml	40 µg/ml	20 µg/ml	2 µg/ml	0.2 µg/ml	0.02 µg/ml	blank
abs1	1.235	0.241	0.244	0.33	0.333	0.803	0.982	0.244
abs2	1.240	0.238	0.248	0.312	0.344	0.777	0.988	0.244
average of absorbance	1.238	0.240	0.246	0.321	0.339	0.790	0.985	0.244
average of absorbance - blank	0.994	-0.005	0.002	0.077	0.095	0.546	0.741	0.000
cell viability %	100	0	0	8	10	55	75	0
cell inhibition %	0	100	100	92	90	45	25	100

Table A.6: *Cell Viability and Inhibition of HeLa Cells Treated with Varying Concentrations of DOXO from Cell-Hydrazone. Values represent a single experiment performed in duplicate.*

HeLa								
	negative control	80 µg/ml	40 µg/ml	20 µg/ml	2 µg/ml	0.2 µg/ml	0.02 µg/ml	blank
abs1	0.952	0.240	0.277	0.287	0.282	0.668	0.847	0.244
abs2	0.927	0.257	0.275	0.286	0.291	0.662	0.891	0.244
average of absorbance	0.940	0.249	0.276	0.287	0.287	0.665	0.869	0.244
average of absorbance - blank	0.696	0.005	0.032	0.043	0.043	0.421	0.625	0.000
cell viability %	100	1	5	6	6	61	90	0
cell inhibition %	0	99	95	94	94	39	10	100

Table A.7: *Cell Viability and Inhibition of MCF-7 Cells Treated with Varying Concentrations of DOXO from Cell-Hydrazone. Values represent a single experiment performed in duplicate*

MCF-7								
	negative control	80 µg/ml	40 µg/ml	20 µg/ml	2 µg/ml	0.2 µg/ml	0.02 µg/ml	blank
abs1	1.478	0.244	0.251	0.29	0.314	1.296	1.345	0.244
abs2	1.487	0.246	0.255	0.3	0.333	1.245	1.341	0.244
average of absorbance	1.483	0.245	0.253	0.294	0.324	1.271	1.343	0.244
average of absorbance - blank	1.239	0.001	0.009	0.050	0.080	1.027	1.099	0.000
cell viability %	100	0	1	4	6	83	89	0
cell inhibition %	0	100	99	96	94	17	11	100

Table A.8: *Cell Viability and Inhibition of LX-2 Cells Treated with Varying Concentrations of DOXO from Cell-Hydrazone. Values represent a single experiment performed in duplicate.*

LX-2								
	negative control	80 µg/ml	40 µg/ml	20 µg/ml	2 µg/ml	0.2 µg/ml	0.02 µg/ml	blank
abs1	1.108	0.286	0.389	0.42	0.515	0.676	0.711	0.244
abs2	1.105	0.279	0.396	0.46	0.511	0.666	0.715	0.244
average of absorbance	1.106	0.283	0.393	0.439	0.513	0.671	0.713	0.244
average of absorbance - blank	0.862	0.039	0.149	0.195	0.269	0.427	0.469	0.000
cell viability %	100	4	17	23	31	50	54	0
cell inhibition %	0	96	83	77	69	50	46	100

Appendix B

Figures

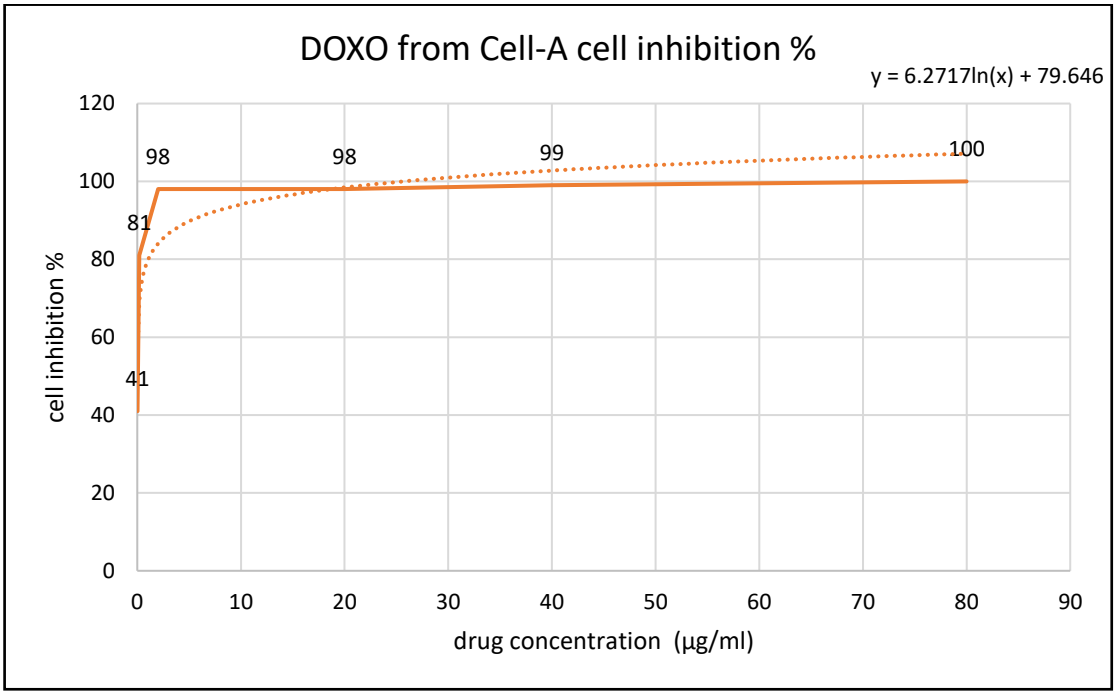

Figure B.1: *Dose-Response Curve of DOXO from Cell-A on HepG-2 Cell Inhibition.*

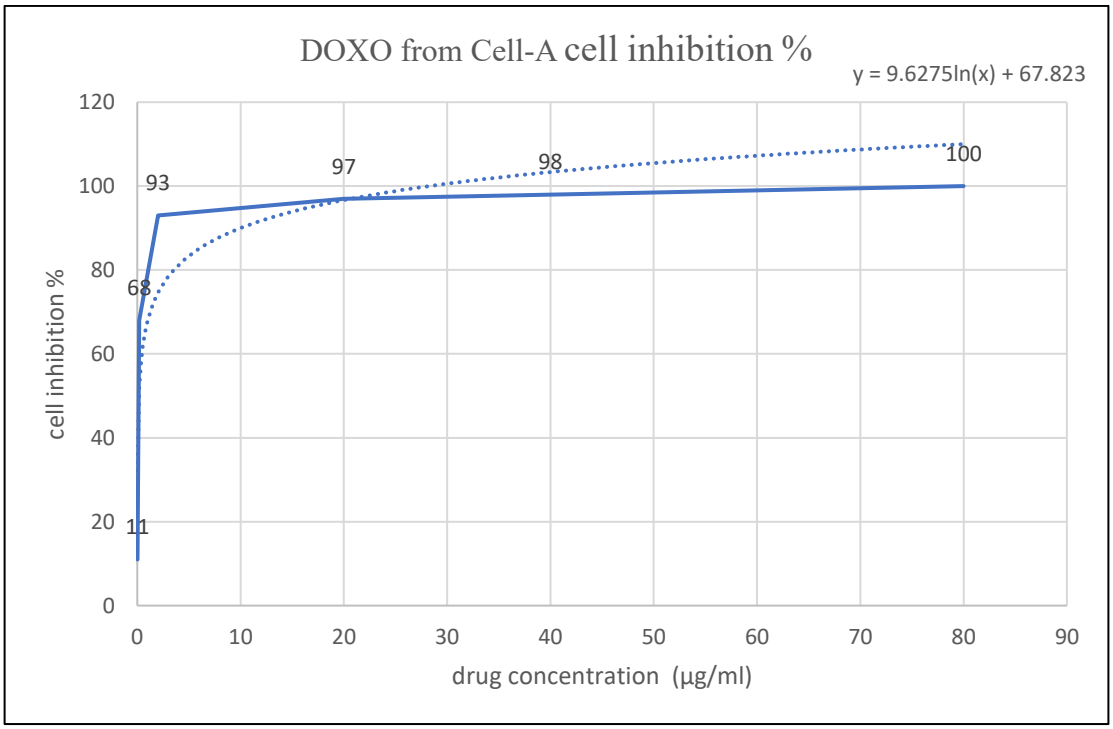

Figure B.2: *Dose-Response Curve of DOXO from Cell-A on HeLa Cell Inhibition.*

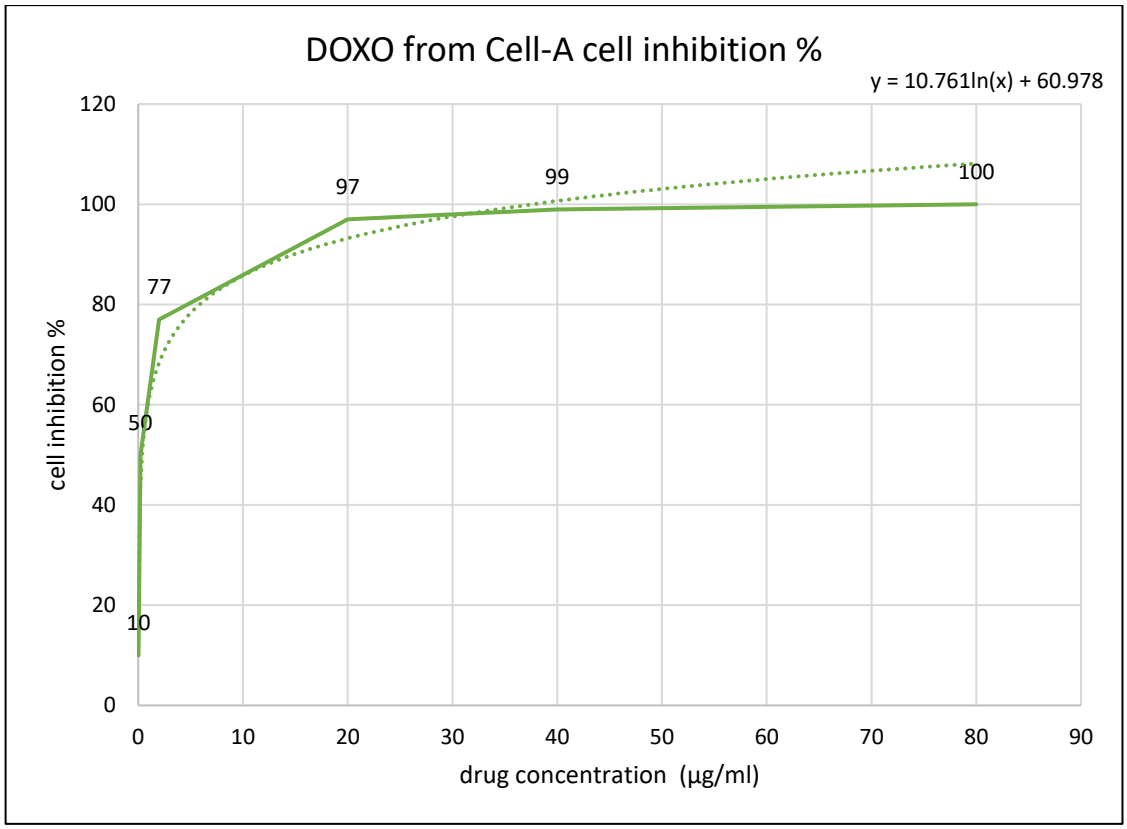

Figure B.3: *Dose-Response Curve of DOXO from Cell-A on MCF-7 Cell Inhibition.*

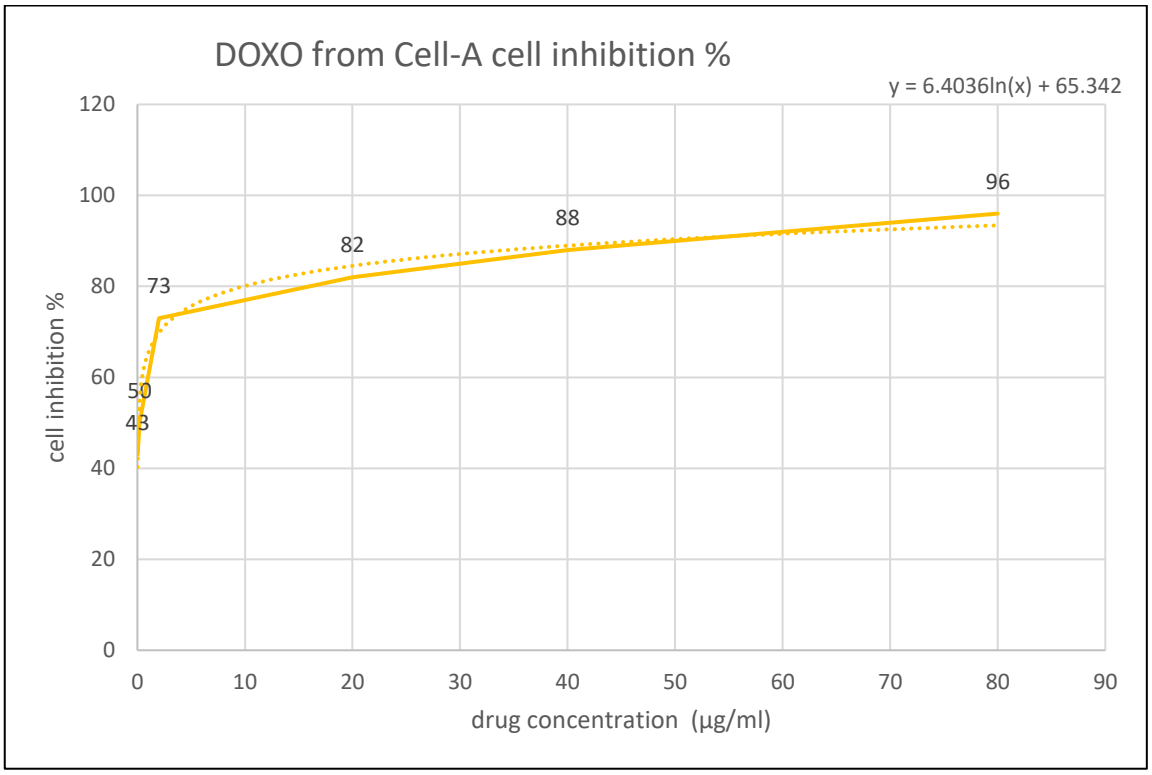

Figure B.4: *Dose-Response Curve of DOXO from Cell-A on LX-2 Cell Inhibition.*

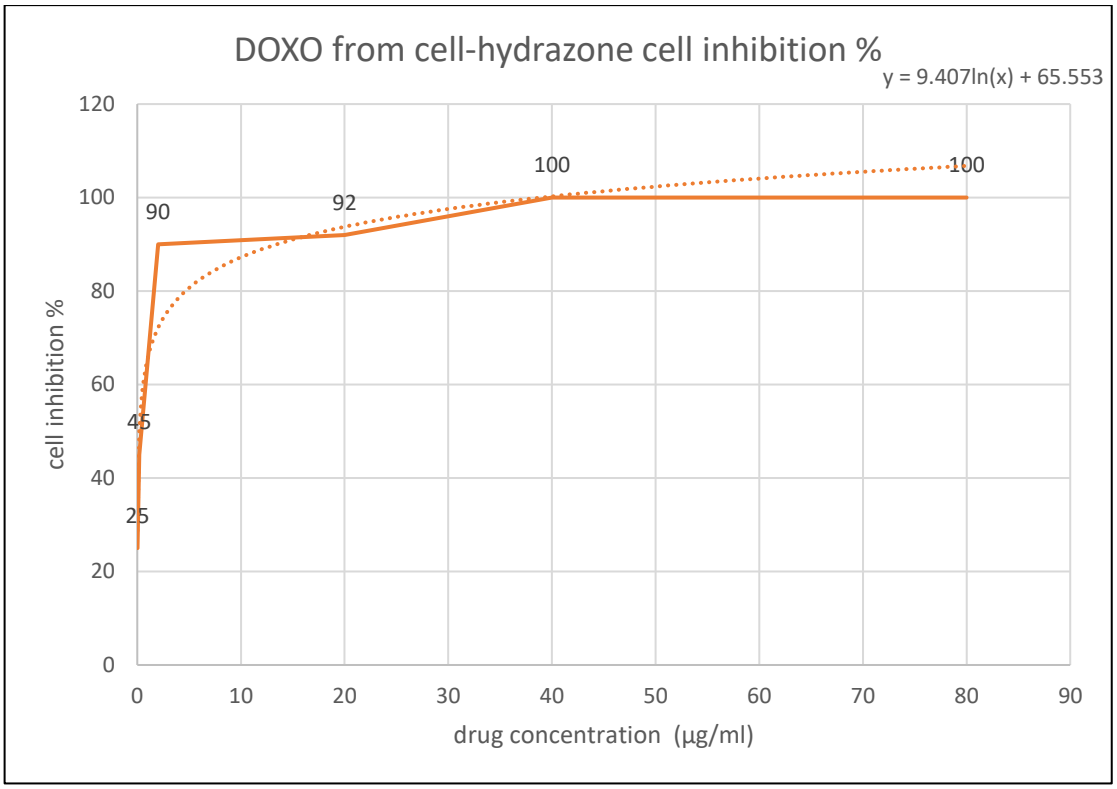

Figure B.5: *Dose-Response Curve of DOXO from Cell-Hydrazone on HepG-2 Cell Inhibition.*

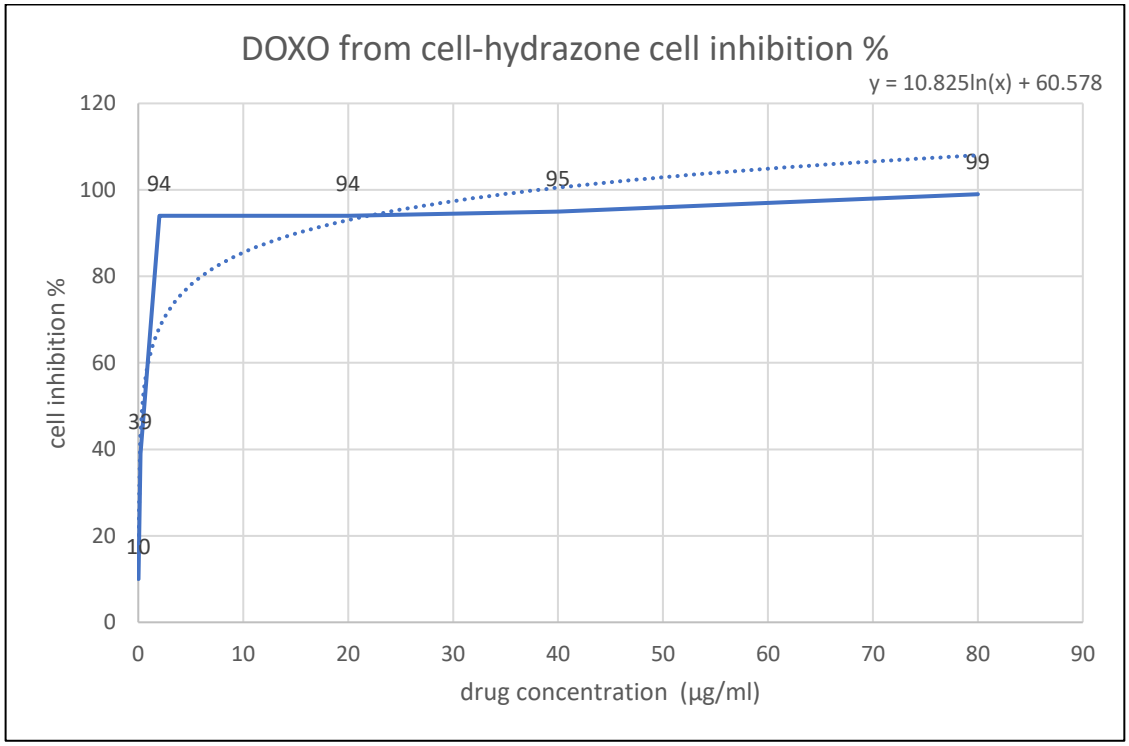

Figure B.6: *Dose-Response Curve of DOXO from Cell-Hydrazone on HeLa Cell Inhibition.*

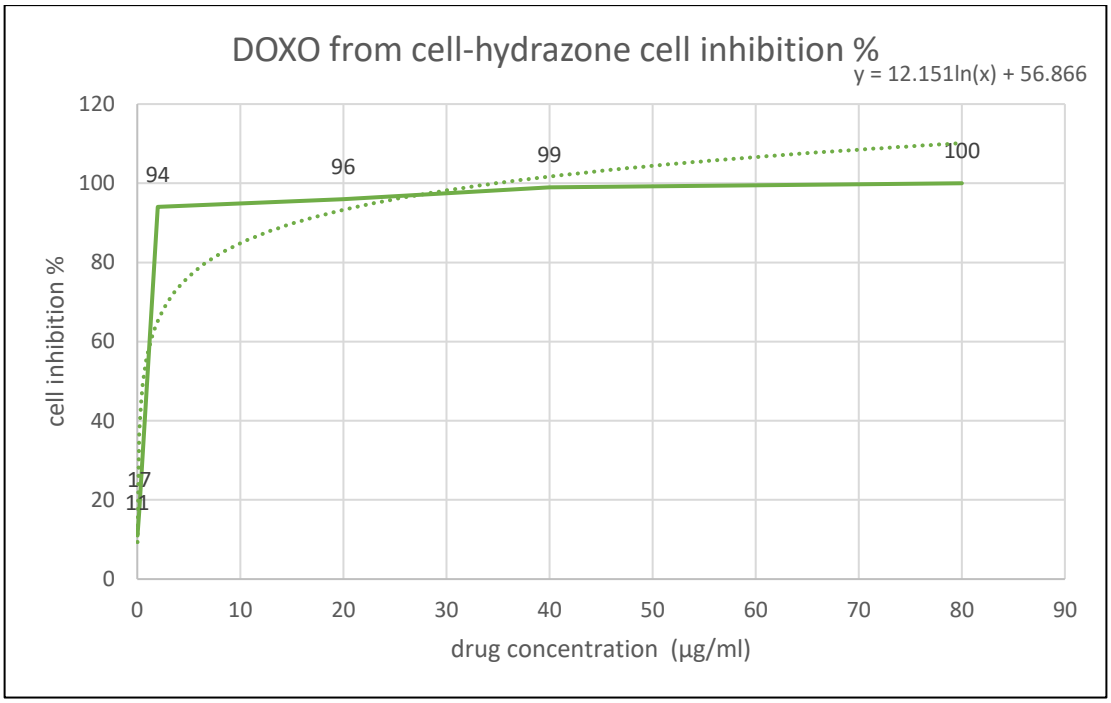

Figure B.7: *Dose-Response Curve of DOXO from Cell-Hydrazone on MCF-7 Cell Inhibition.*

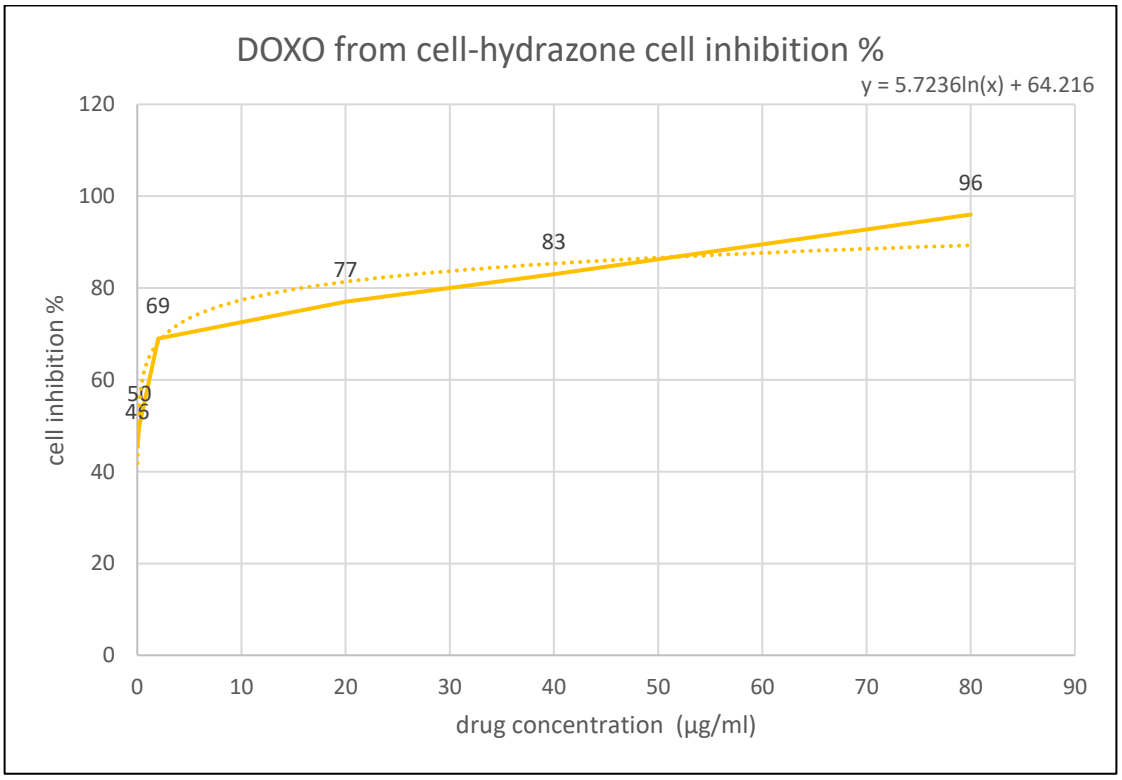

Figure B.8: *Dose-Response Curve of DOXO from Cell-Hydrazone on LX-2 Cell Inhibition.*

جامعة النجاح الوطنية
كليَّة الدّراسات العليا

جسيمات نانوية من السليوز معدلة بالسيستين كنظام توصيل محكم للدواء المضاد للأورام دوكسوربيسين

إعداد
معتصم عزام أحمد فار

إشراف
أ. د. عثمان حامد
أ. د. محي الدين العسالي

قدمت هذه الرسالة استكمالاً لمتطلبات الحصول على درجة الماجستير في الكيمياء بكلية الدراسات العليا في جامعة النجاح الوطنية في نابلس، فلسطين.

2026

جسيمات نانوية من السليوز معدلة بالسيستين
كنظام توصيل محكم للدواء المضاد للأورام دوكسوربيسين

إعداد

معتصم عزام أحمد فار

إشراف

أ. د. عثمان حامد

أ. د. محي الدين العسالي

الملخص

تناولت هذه الدراسة تطوير وتوصيف أنظمة توصيل مستجيبة للرقم الهيدروجيني مشتقة من بوليمرات السيليلوز المعدلة لاستخدامها في العلاج الموجه للسرطان. تم تنشيط السليلوز ذو البلورات الميكروية باستخدام نظام كلوريد الليثيوم المذاب في الدايميثيلاسيتاميد، ثم عدل كيميائيا لإنتاج وسائط رئيسية مثل توسيلات السيليولوز والسليلوز ثنائي الألدهيد، تم دمج مجموعات وظيفية مختلفة تشمل إل–سيستين والملامين والباي–فينيلين ديامين، والهيدرازين لإنتاج سلسلة من النواقل المتخصصة. وأكدت تحاليل مطيافية الأشعة تحت الحمراء نجاح هذه التعديلات من خلال ظهور مجموعات الثيول، والأمين، والإيمين

أظهرت النتائج أن الجسيمات النانوية لـ سليلوز–سيستين المحملة بالكيرسيتين امتلاكها قطراً يتراوح بين 70–90 نانومتر وجهد زيتا يبلغ –28 ملي فولت، مما يشير إلى استقرار إلكتروستاتيكي جيد ومنع التكتل. وبلغت كفاءة تحميل الكيرسيتين على الناقل 17.04%. كشفت دراسات قياس التحرر للدواء من داخل شبكة البوليميرات المعدلة عن سلوك يعتمد بشكل كبير على الرقم الهيدروجيني؛ حيث كان معدل تحرر الكيرسيتين من سليلوز–سيستين عند الرقم الهيدروجيني 7.4 (الفسيولوجي) أقل بـ 70 مرة مقارنة بمعدل التحرر عند الرقم الهيدروجيني 6.5 (الوسط الحمضي للأورام).

كما أظهرت أنظمة السليلوز ثنائي الألدهيد والسليلوز–هيدرازون تحرراً متسارعاً لعقار الدوكسوروبيسين في الظروف الحمضية نتيجة أيونات الهيدروجين الموجبة الى الروابط الكيميائية وزيادة انتفاخ البوليمر.

وفي اختبارات السمية الخلوية، أظهر عقار الدوكسوروبيسين المحرر من ناقل السيليلوز ثنائي الالدهيد فعالية استثنائية ضد خط خلايا سرطان الكبد (HepG-2) بتركيز مثبط نصفي (IC50) قدره 0.0089 ميكروغرام/مل، وهو ما يطابق تقريباً فعالية الدواء الحر كما تم تحقيق تثبيط للخلايا بنسبة تصل إلى 100% في عدة خطوط خلوية تشمل HeLa و MCF-7 عند التركيزات العالية.

تشير هذه النتائج إلى أن نواقل السليلوز النانوية المعدلة توفر منصة مستقرة وحيوية وفعالة للغاية للتحرر المنضبط والمحفز للأدوية المضادة للسرطان، مما يقلل من الآثار الجانبية على الأنسجة السليمة.

الكلمات المفتاحية: السليلوز، السليلوز المُعدَّل بالسيستئين، الجسيمات النانوية، نظام توصيل الدواء، الإطلاق المتحكم فيه للدواء، إطلاق الدواء المستجيب للرقم الهيدروجيني (pH)، دوكسوروبيسين، علاج السرطان، رابطة هيدرازون، النواقل النانوية.